An Experimental Study of Contactless Respiration Rate Estimation Using Millimeter-wave FMCW Radars

Semih Iseri

Master's Thesis
UNIVERSITY OF HELSINKI
Department of Computer Science

Helsinki, November 4, 2020

HELSINGIN YLIOPISTO — HELSINGFORS UNIVERSITET — UNIVERSITY OF HELSINKI

Tiedekunta — Fakultet — Faculty	Laitos — Institution — Department
Faculty of Science	Department of Computer Science

Tekijä — Författare — Author

Semih Iseri

Työn nimi — Arbetets titel — Title

An Experimental Study of Contactless Respiration Rate Estimation Using Millimeter-wave FMCW Radars

Oppiaine — Läroämne — Subject

Computer Science

Työn laji — Arbetets art — Level	Aika — Datum — Month and year	Sivumäärä — Sidoantal — Number of pages
Master's Thesis	November 4, 2020	44

Tiivistelmä — Referat — Abstract

Sleep is a very integral part of human life. Our happiness and overall productivity greatly depend on how well we sleep. It is even more important for kids and babies as it directly affects growth and future well being. Today, it is possible to use a variety of devices to monitor sleep duration and sleep quality, helping us improve how well we sleep. However, most common sleep tracking methods require wearing an electronic device, e.g. a smartwatch or a smart bracelet, to monitor vital signs, and sleep quality information is estimated based on this information. Wearing a watch or a bracelet while sleeping is, however, considered uncomfortable by many and may not be applicable for babies.

In this thesis, we study a non-invasive method for measuring the respiration rate to be used for sleep monitoring. We aim to obtain the breathing rate of an individual with no contact. We use a frequency-modulated continuous-wave radar to track chest movements and estimate the breathing rate from this signal. We use the phase component of the raw radar signal in the frequency domain to emphasize the small movements and autocorrelation function to detect the periodicity of the signal.

During the study, we carried out an experiment, and we have compared our method to a traditional vital sign measurement device, and we found that our method matches the performance of the commercial device for breathing rate measurement, and outperforms it when it comes to comfort and practicality. Although it may be necessary to collect more data to better verify our results, the outcome of the experiment indicates that this method can provide the needed vital sign measurement performance without being invasive, i.e. without needing to wear any electronic devices.

Avainsanat — Nyckelord — Keywords

radar, respiration rate, sleep analysis, signal processing

Säilytyspaikka — Förvaringsställe — Where deposited

Muita tietoja — Övriga uppgifter — Additional information

Contents

1 Introduction

Health monitoring devices have been around us for more than a hundred years. If we think of the thermometer as the first health monitoring device, it was invented in 1592 by Galileo Galilei, but it took over a century for its widespread adoption for patient monitoring [37]. Similarly, if we consider electrocardiography as the first electrical sensor, invented in the early 20^{th} century, we can easily say that health monitoring devices have been around us for over a century. However, it was not until very recently that commercial health monitoring devices became accessible for the general public.

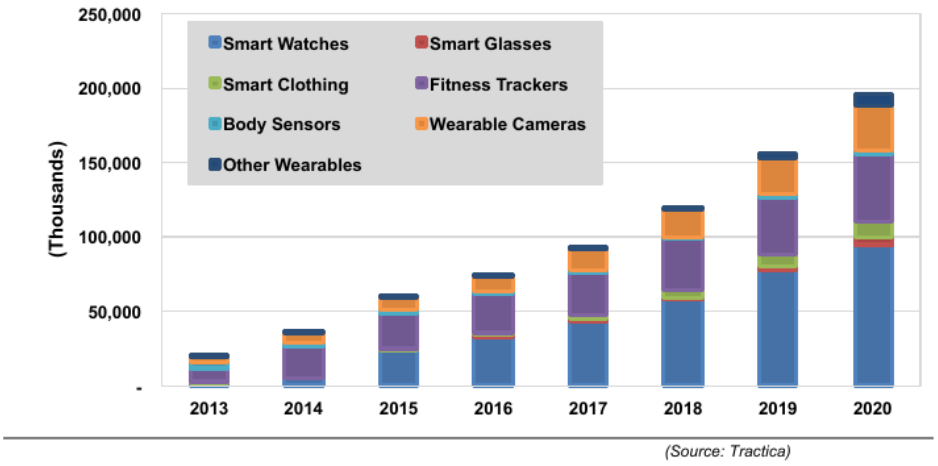

Figure 1: Wearable Device Shipments by Device Type, World Markets: 2013-2020 [20]

As technology gets more and more accessible, an ever-increasing number of people have started buying health monitoring devices for their everyday use. As can be seen in Figure 1, the sales of wearable sensors are steadily increasing, and it is estimated that in 2020 nearly $150 million worth of wearable sensors will be sold.

In order to counter the demand and increase their market shares, manufacturers are coming up with new devices for different purposes and also in different form factors. The range goes from activity-tracking smart rings to advanced smartwatches that can also act as a sensor hub to connect to other external sensors. Some of these devices are intended to track general activity. For example, a basic wristband can estimate how many steps have been taken during a day and estimate how many calories were burned. More advanced sensors, however, can be connected to external sensors and generate a broader set of data during an exercise. For example, a smartwatch, coupled with cadence and speed sensors, could estimate the amount of energy burned during the trip, as well as the distance traveled and give tips on improving

Figure 2: An arrangement of sensors: Beddit Smart Sleep Tracker, Oura Smart Ring, Suunto Bluetooth LE HRM, and Suunto Ambit 3 smartwatch.

exercise quality.

One particular application for these sensors is sleep tracking. Wearable devices such as heart rate belts, smart wristbands, or smartwatches can monitor changes in heartbeat rate and combine it with movement to make estimations about sleep state and sleep quality [31]. However, wearing a device during sleep could compromise comfort.

Not all sleep monitors are wearables, and not all sleep monitors are invasive. For example, some sensors, such as Beddit Sleep Monitor [1], can be placed between the mattress and bedding. They typically gather respiration and movement data from the pressure changes, which are later interpreted to obtain sleep data. As a downside, these sensors require to be placed precisely at chest level, and this requirement makes them unfit especially for those who move around their bed while sleeping [2].

While many practical products are used by adults, the need for sleep monitoring is not exclusive for an age group. For example, there are special products which are designed to monitor babies' sleep, such as Owlet [13] and Nanit [10] baby monitoring systems. However, different constraints apply for a baby focused sleep monitoring device, and surely the most important constraint is safety. There are different safety requirements in different countries, but, as an example, it is usually deemed unsafe to have a loose belt or a loose cord [5] in a baby cot because this can potentially entangle

the baby, very likely blocking block blood flow or airflow, causing life-long injuries or even death. Another possible safety hazard is small parts [16]. It is possible for a small object to choke the baby, resulting in death. As a result, it is widely suggested to have nothing in a baby crib other than the baby and a mattress [8].

This thesis builds on the idea of creating a robust non-invasive sleep monitoring solution, mainly for babies, using VTT's state-of-the-art 24GHz frequency-modulated continuous-wave radar [29]. The radar can detect tiny movements of the human body without contact, even those caused by heartbeats, and through many types of materials such as fabrics. It can be placed away from the baby, possibly under the crib or on top of the crib, yet it can still provide necessary data to estimate sleep quality.

Although the ultimate goal is to create a product to monitor baby sleep, it is deemed too broad for a thesis due to both technical and ethical difficulties in collecting data. Instead, we will focus on the technical question of estimation of respiration rate using the radar, and we will do this for adults. Sleep quality can later be estimated based on this data [26]. At the end of this process, we are aiming to get sufficient information about the general feasibility of this approach to be used for designing the follow-up studies to progress towards the eventual goal of monitoring baby sleep.

The thesis is structured in a logical way. We will first start with the necessary background information (Chapter 2). In this part, we will be describing the devices and techniques that we are going to utilize later in the text. Later, we will describe the signal processing pipeline (Chapter 3) and the experiment setup (Section 4.1). Then we will look at the data and see its performance against a commercial solution (Section 4.4). And finally, we will wrap up and conclude the thesis in Chapter 5.

1.1 Related Work

Before starting to study feasibility of using an FMCW radar to measure respiration rate to be used for sleep monitoring, we looked for similar work. In other words, we searched for other studies where a radar is used for sleep monitoring or measuring vital signs. In the end, we have collected a handful of relevant research papers and we would like to discuss about them here.

Movement and Respiration Detection using Statistical Properties of the FMCW Radar Signal [30] In this paper, Kiuru et al. have used the same radar hardware that is used in this thesis to detect movement and respiration. However, this study only investigates detecting whether there is a movement or respiration. It does not try to measure the amount of movement or the respiration rate.

DoppleSleep: A Contactless Unobstrusive Sleep Sensing System Using Short-Range Doppler Radar[40] In this paper, Rahman et al. have compared the performance of a doppler radar against multiple off-the-shelf sensors for monitoring sleep quality as well as the vital signs. Although the paper features a radar with a different working principle, the end goals are very similar to this thesis. On the other hand, the work in the paper has a wider scope than this thesis: It includes the measurement of respiration rate, heart rate, and sleep quality, whereas we have only focused on the measurement of the respiration rate. Moreover, it features a standalone measurement device prototype as well as a mobile application to interact with it.

Smart Homes that Monitor Breathing and Heart Rate[22] In this paper, Adib et al. uses an FMCW radar to detect the respiration rate, and heart rate to be used in a smart home. This work aims to obtain these vital signs regardless of the position of the subject inside a room, even when it is occupied by multiple people. This paper also includes comparisons of this system against an off-the-shelf vital sign measurement device.

The use of FMCW radar as well as the approach show great similarities to this thesis. However, the paper deals with slightly different constraints compared to this thesis such as multiple targets in the range and variable distance between the radar and the test subject.

Assessment of Human Respiration Patterns via Noncontact Sensing Using Doppler Multi-Radar System [27] In this article, Gu et al. uses multiple doppler radars to demonstrate the chest movement patterns in different conditions such as when the person is angry, or when the person is reading a text as well as when the person is not breathing. Although the paper features a different kind of a radar than what we have used, the presentation of the respiration patterns in different human conditions make it very important to understand how chest movements appear on radar. Thus, making it very relevant for accurate respiration rate measurement, which is one of the end goals of this thesis.

2 Background

As briefly summarized in Chapter 1, the process described in this thesis involves several steps, which might not be familiar to the reader. This chapter intends to give sufficient background information so that the entire process can be understood clearly.

2.1 Frequency-Modulated Continuous-Wave (FMCW) Radar

RADAR is an abbreviation for **ra**dio **d**etection **a**nd **r**anging. As the name implies, it is a technique that uses the reflected radio waves to detect objects, and their position, speed, etcetera. The concept of *RADAR* itself is vast since there are multiple different types of radars with different working principles. We have used an FMCW radar in this thesis, and we see it necessary to explain how it works. Thus, we will be describing the operation from very low-level concepts to higher. For a general overview of radars, see the online lectures made by IEEE Aerospace and Electronic Systems Society and IEEE New Hampshire Section [35] or the coursebook Introduction to Radar Systems written by Merrill I. Skolnik[42].

We will start from the name and then continue with the basic building block of the FMCW radar, namely the *chirp*. Later, we will analyze the transmitted and received signals and then continue with a glimpse of the mathematics of signal theory and how it applies to our application with FMCW radar. Finally, we will discuss VTT's 24 GHz FMCW radar and its parameters.

2.1.1 Frequency Modulation

Before starting with frequency modulation, it is essential to discuss modulation itself and why we modulate signals. Modulation is an operation during which a signal is embedded into another signal named *carrier*. This involves the modification of the carrier signal based on the input signal. For example, amplitude modulation (AM) alters the amplitude of the carrier signal. Similarly, frequency modulation (FM) alters the frequency of the carrier signal. Figure 3 illustrates these two modulation types for a better understanding.

This process has many practical uses. For example, it enables long-distance voice transfer over the air. Normally human voice cannot be transmitted far; the farthest recorded propagation of human voice, as is, is 180 meters as of 2020 [7]. However, when it is modulated using an HF carrier signal [11], which can be reflected off the ionosphere, it can reach over the horizon and travel greater distances [34]. As another example, modulation is used when multiple signals need to share the same transmission medium. The signals can be modulated over different carrier signals at the source,

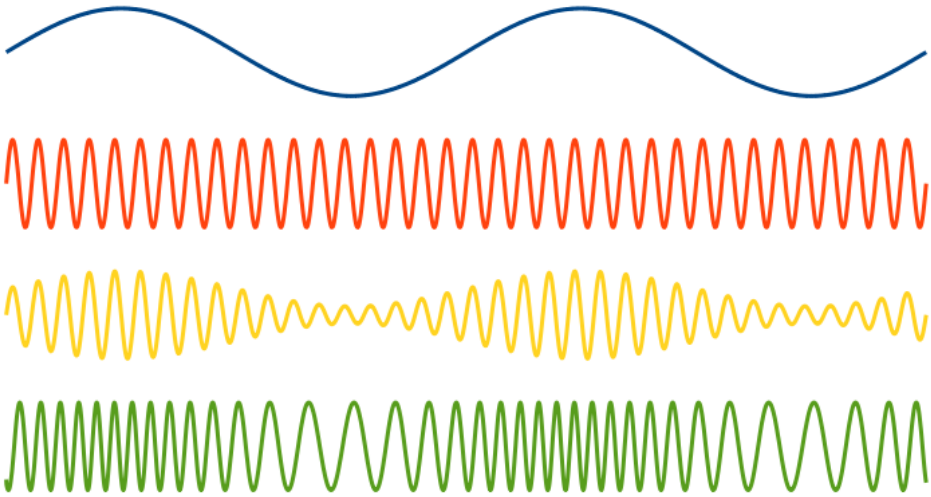

Figure 3: Base signal and different modulations. From top to bottom: The original signal, the carrier signal, the amplitude modulated signal, and the frequency modulated signal. Typically, the original signal is at a significantly lower frequency than the carrier signal. With amplitude modulation, the amplitude of the carrier signal is modified in accordance with the input signal. With frequency modulation, the frequency of the carrier signal is modified in accordance with the input signal. In this example, carrier frequency decreases as the input signal decreases, and it increases as the input signal increases. Please note that the effects of the input signal on the output signals are exaggerated in this plot for better visualization.

and they can be separated at the destination by their carrier frequencies. One very common application of this process is, e.g., terrestrial radio and television broadcast. Different entities use different *channels* to broadcast their programs over the air. In this case, the air is the shared medium, and a *channel* is nothing but its carrier frequency. The consumers of the signal, the *receivers* can pick their desired source by filtering out the other carrier frequencies.

2.1.2 Chirp

Radars work by emitting radio signals and receiving them back. Even though they all emit radio signals, they emit different kinds of signals and work based on different principles. For example, pulse radars transmit a short pulse and observe how long it takes for the signal to come back. On the other hand, doppler radars emit continuous radio waves at a constant frequency and observe the frequency shift of the reflected signal. As a result of their

operation principle, for example, doppler radars cannot tell the distance of the target, or pulse radars can only work in longer distances [24].

FMCW radar works differently. It works by observing the delay of the transmitted signal, similar to a pulse radar, but it emits a continuous wave, similar to a doppler radar. But unlike a doppler radar, it emits a variable frequency signal. This signal is called *chirp*. CHIRP is an abbreviation of **c**ompressed **h**igh-**i**ntensity **r**adar **p**ulse, and it is essentially an FM modulated signal that could be triangular, sawtooth, or even sinusoidal shaped. Since VTT's radar uses a sawtooth-shaped signal, we will be focusing only on the sawtooth-shaped chirp in this thesis.

The chirp fixes the range problem of the pulse radar as it allows for shorter range distance measurement, and it increases the range resolution while keeping the power consumption low [23]. Moreover, similar to Doppler radar, it allows monitoring of the phase shift for detecting very small movements. These features make the FMCW radar suitable for our application, and we think that it is very important to understand how it works in order to grasp the technical explanations later in this thesis.

On a very basic level, FMCW radar works by comparing the received signal to the transmitted signal. To be more precise, it compares the instantaneous frequency of the received signal to the instantaneous frequency of the transmitted signal. We can calculate the range of the object from this comparison, and we can apply further signal processing to get the relative velocity of the object. However, this requires a better technical understanding of the chirp.

As a continuous-wave radar, FMCW radar emits a series of chirps. However, for the sake of simplicity, we will use a single chirp for the rest of the explanation. Figure 4 depicts a single chirp. This signal can be defined by its starting frequency f_c, its duration T_c, and its bandwidth B. And we can also calculate the slope of the chirp S using

$$S = \frac{B}{T_c}.$$

Let us assume there is an object in front of the radar, with a distance d between the object and the radar. The object reflects some of the signals back to the radar, which would then get picked up by the antenna and get amplified. When we plot both the transmitted and received signals on the same graph, we get the upper plot shown in Figure 5. From this figure, we can calculate the distance between the object and the radar using

$$d = \frac{\tau \times c}{2},$$

where c is the speed of light and τ is the time shift between the transmitted and received signal, as shown in Figure 5.

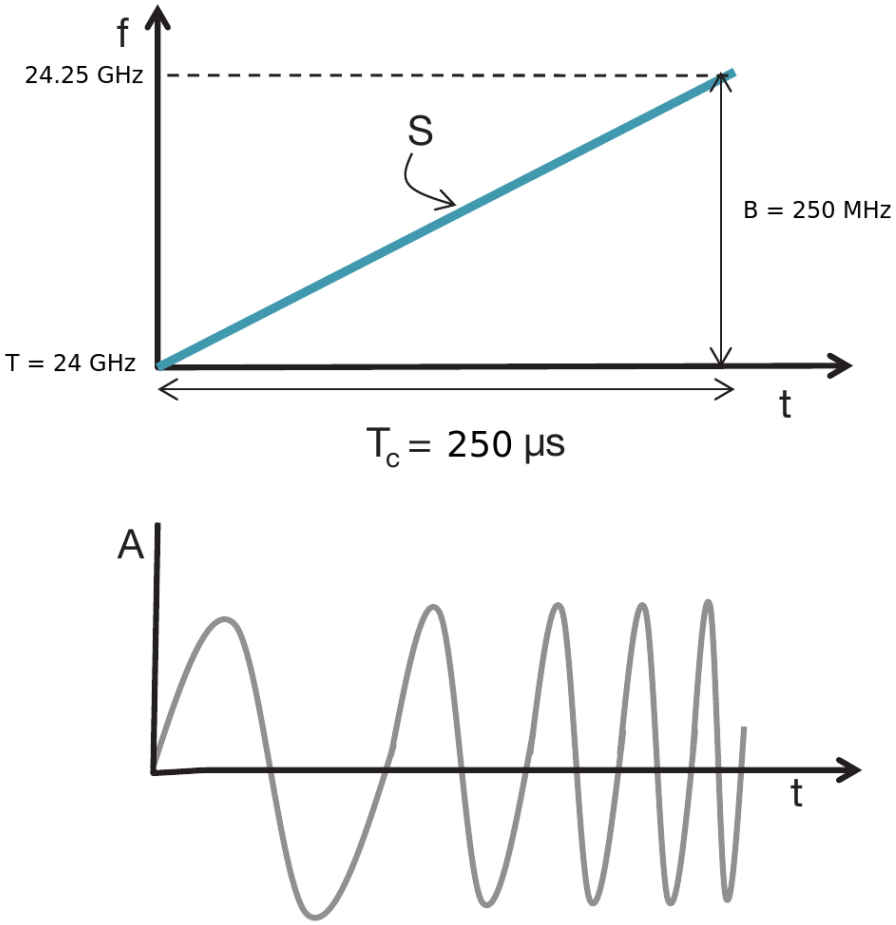

Figure 4: Top: Frequency versus time graph of the chirp used by VTT radar. Bottom: Amplitude versus time graph of a chirp. Note that the frequency change is exaggerated in the bottom graph. Source: [25]

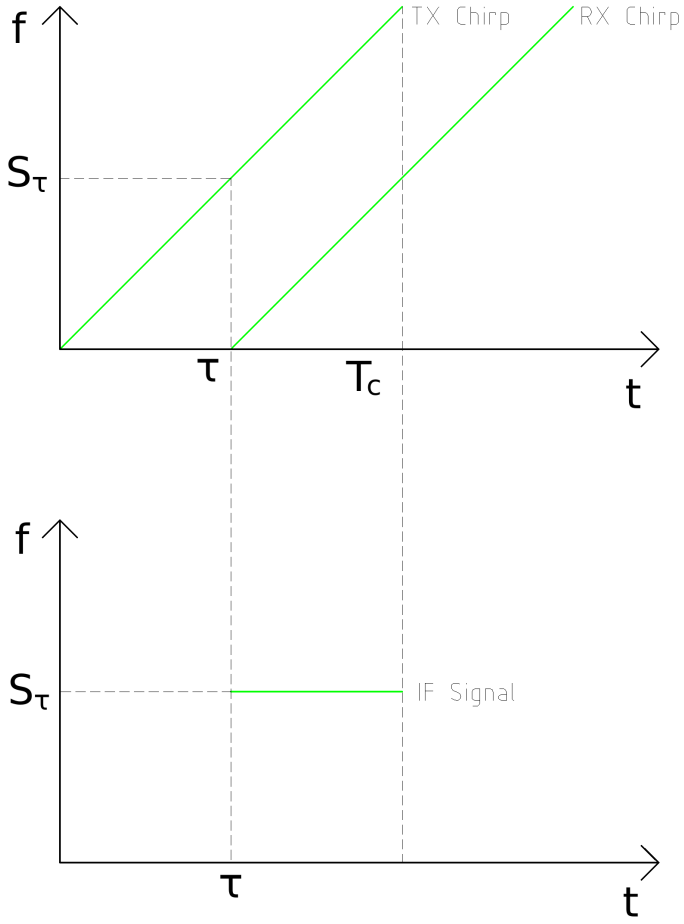

Figure 5: Top: Frequency versus time graph of both transmitted and received signals. Bottom: Frequency versus time graph showing Intermediate Frequency (IF) signal. This signal is the output of the mixer when TX and RX signals are given as input.

However, determining τ is a difficult step since it requires sampling of a very high-frequency signal. Sampling and then digitally processing such signals require expensive equipment. However, by using circuitry, as shown in Figure 6, we can obtain frequency difference f_d and calculate the distance from there.

The critical component of this block diagram is the mixer denoted with the symbol shown in Figure 7. This device can add or subtract signals in the frequency domain. Thanks to it, we can work on a lower frequency signal. By using the input signals x_1 and x_2 as defined in Equations (1) and (2), the output signal x_{out}, also known as IF or intermediate frequency, can be

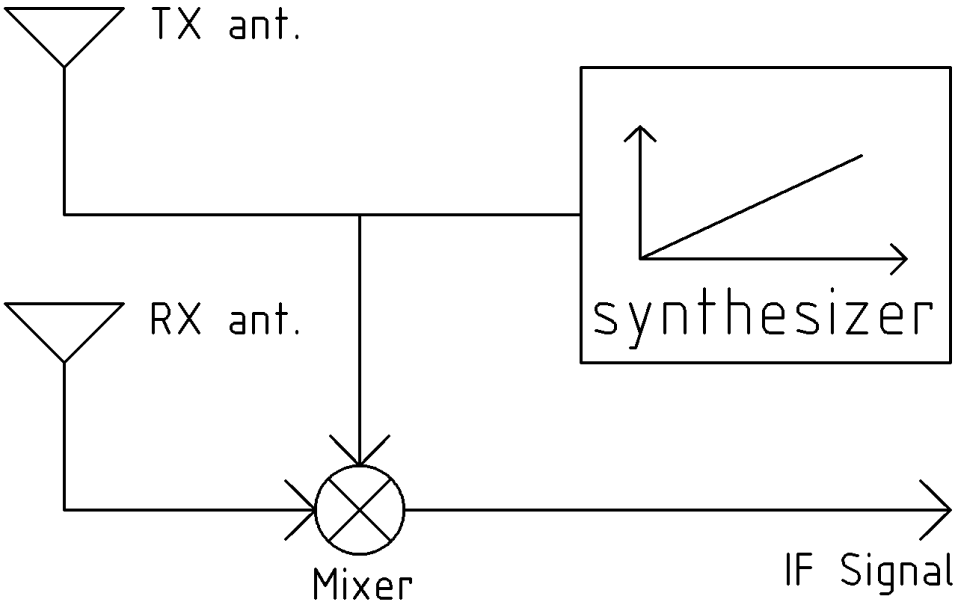

Figure 6: FMCW radar block diagram.

defined as in Equation (3) [25].

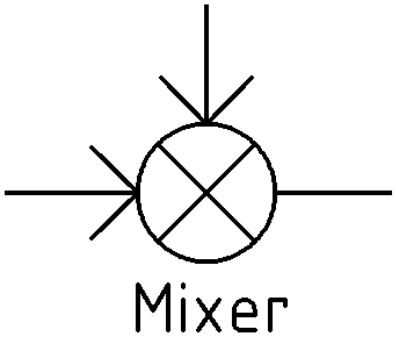

Figure 7: Mixer

$$x_1 = sin(\omega_1 t + \phi_1), \tag{1}$$

$$x_2 = sin(\omega_2 t + \phi_2), \tag{2}$$

$$x_{out} = sin[(\omega_1 - \omega_2)t + (\phi_1 + \phi_2)]. \tag{3}$$

If we assume x_1 is the TX signal and x_2 is the RX signal, we can calculate

the distance d from the Equation (3) using

$$d = \frac{(\omega_1 - \omega_2) \times c}{2 \times S}.$$

Since the output of the mixer is a continuous signal, it needs to be sampled in order to be processed digitally. Sampling converts the continuous signal into a discrete time-series signal, with which the frequency distribution can be obtained using a computational discrete time-series Fourier transform algorithm. We have used FFT, fast Fourier transform, in this thesis. However, before proceeding, it is helpful to look at the general discrete time-series Fourier transform process to have a better understanding of its limitations.

2.1.3 Discrete Time-Series Fourier Transform

All periodic signals can be expressed as an infinite sum of sinusoidal signals. This conversion process is called Fourier Transform and is defined as

$$\hat{f}(\xi) = \int_{-\infty}^{\infty} f(x)\ e^{-2\pi i x \xi}\, dx$$

where $f(x)$ is the signal in the *time domain*, and $f(\xi)$ is the signal in the *frequency domain* [36].

The same transformation can be modified for discrete-time signals. This process is called discrete-time Fourier transform (DTFT) and is defined as

$$X[k] = \sum_{n=0}^{N-1} x[n] e^{-i \frac{2\pi}{N} kn}$$

where N denotes the number of samples, and k is the bin number for a time-domain signal $x[n]$ [36].

From a very high-level perspective, DTFT takes in the discrete signal and outputs a number of *bins* where each bin represents an interval of frequencies. The amount of these bins are determined by the number of samples. The resolution of each bin is dependent on sampling frequency f_s, and the number of samples N. The bin resolution d_b can be calculated as

$$d_b = \frac{f_s}{N}$$

In order to have a better DTFT resolution for lower frequencies, one has to reduce the DTFT resolution. This is done by either reducing the sampling frequency while keeping the number of samples the same or by increasing the number of samples while keeping the frequency the same. However, in our case, both the sampling rate and sample count are fixed in hardware. Therefore, we cannot change the DTFT resolution.

Due to this limitation, we cannot reliably use the bin frequency to detect small movements caused by breathing. However, as can be seen in the Equation 3, movements alter the signal phase as well. Since the DTFT process outputs complex numbers, it is possible to calculate the phase and observe the change over time. Unlike bin frequency, the angle changes can be observed at a higher resolution.

The observation of phase provides information on very small movements, and even heartbeat detection seems possible using this data. As a drawback, it only indicates relative movement, and it requires constant monitoring. Otherwise, the movement information can get corrupted due to *phase wrapping*, as described in Section 2.1.4. Big movements, such as those caused by one rotating themself, will also cause the phase to roll over faster than it can be measured, resulting in corruption of the small movement data. Also, the shape of the signal is very complex and not well defined since it depends on constructive or destructive interferences of the signal reflected back by the human body. This prevents us from using simple thresholding or shape matching. But it is possible to compare the signal against itself using *autocorrelation* as described in Section 2.3.2.

2.1.4 Phase Unwrapping

Before starting to explain phase unwrapping, it is essential to shortly describe *phase wrapping*. Phase wrapping is a mathematical phenomenon that happens thanks to the way trigonometry works. Since $f(2\pi) = f(0)$, or more generally $\forall n \in \mathbb{Z} \quad f(n*2\pi) = f(0)$ for a trigonometrical function f (e.g. $sin(x)$, $cos(x)$ etc.), it is not possible to distinguish the actual angular distance. As a result, inverse trigonometric functions can only give angular displacement. This output is usually between 0 and 2π or $-\pi$ and π. This phenomenon is called phase wrapping. See Figures 8 and 9 for a visual explanation.

Phase unwrapping is a method to correct this phenomenon. However, it only works if the angular speed is slow enough. For example, Python module NumPy unwrap() function assumes that the phase can move only less than *pi* between two data points [12]. In this case, if the phase moves more than π, then the unwrapped phase will no longer be correct. See Figures 8 and 9 for a visual explanation.

2.1.5 VTT Radar Hardware

We used a small and self-contained 24 GHz FMCW radar module for the experiments conducted for this thesis. This radar, which can be seen in Figure 10, is developed by VTT, Technical Research Centre of Finland, as a general-purpose radar to be used in various industries, including robotics, security, and medical [29]. While it is mostly used for research purposes, several productization ideas are also being investigated in parallel. For

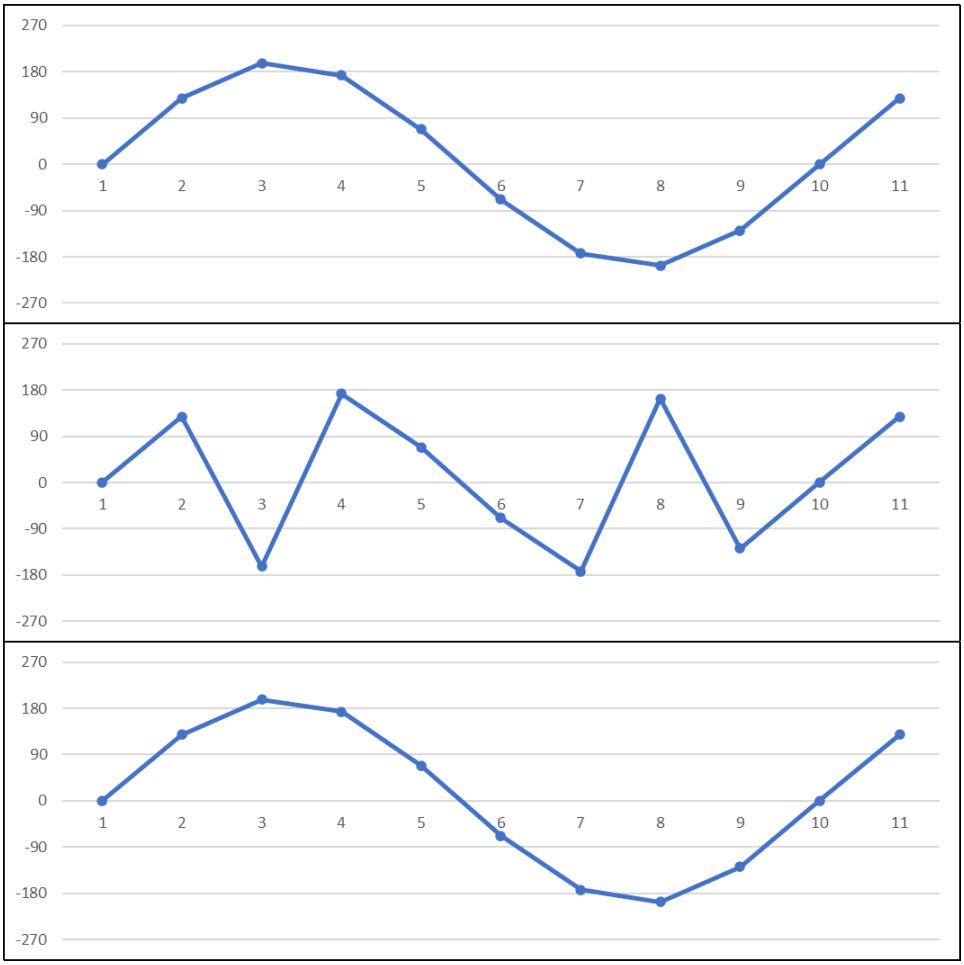

Figure 8: Phase wrapping and unwrapping process for $phase = 200sin(40x)$. From top to bottom: Original signal, wrapped signal, unwrapped signal. Note that all the points in the middle chart are between -180°and 180°

example, Guidesense [6] project uses this radar module to aid the visually impaired. Another example is, of course, the baby sleep monitor idea that gave birth to this thesis.

A list of basic parameters of the radar is illustrated in Table 1 and more can be read in the cited paper written by Jardak et al. [29].

2.2 Human Respiration

Respiration is one of the most important functions of life. A human can survive only a few minutes without breathing. Thus it is one of the first things paramedics try to recover when they engage in an emergency. The process of breathing is to deliver atmospheric oxygen to the cells and the

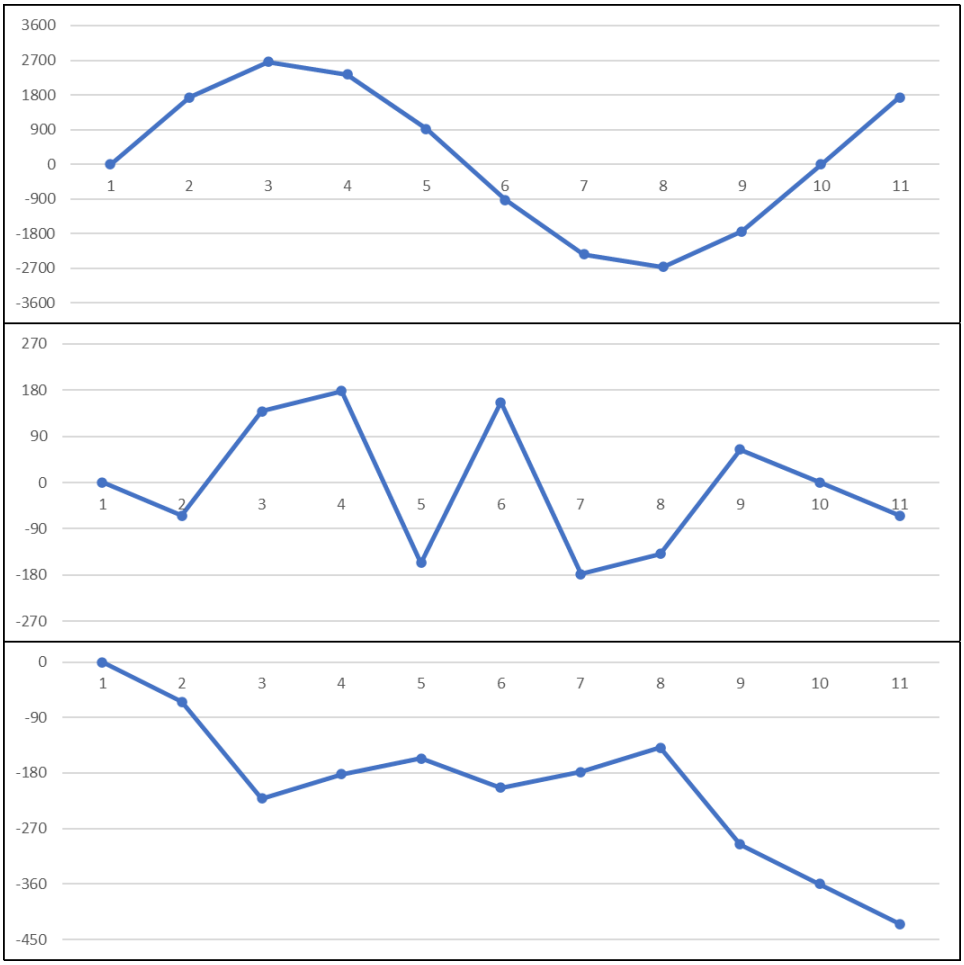

Figure 9: Phase wrapping and unwrapping process for $phase = 2700sin(40x)$. From top to bottom: Original signal, wrapped signal, (incorrectly) unwrapped signal. Note that all the points in the middle chart are between -180°and 180°. Also, note that the signal in the bottom chart is very different from the original signal. This happened because the change between data points was greater than 180°.

System Parameters	Value
Pulse duration: τ	$250\mu s$
Bandwidth: β	$250MHz$
Range resolution: $\triangle R$	$0.6m$
Sampling frequency: f_s	$500KHz$
FFT Size	512

Table 1: Parameters of VTT's radar

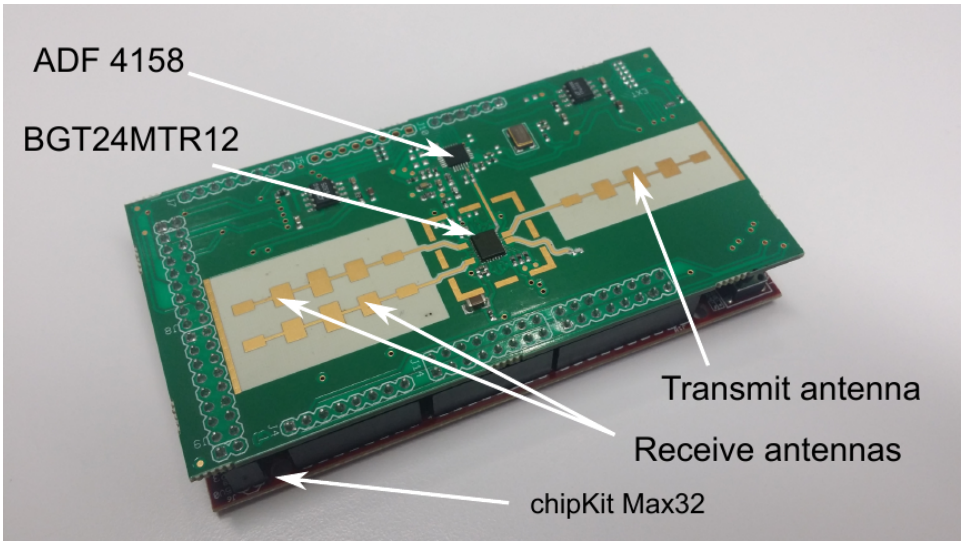

Figure 10: A photo of VTT's 24GHz FMCW radar

metabolical carbon dioxide back to the atmosphere. The entire process is very complicated, and it is mostly out of the scope of this thesis. However, we are interested in the mechanics of breathing, as our measurement technique relies on it. Therefore, we will be explaining the mechanical part of the breathing process from a high-level point of view, following the presentation in [28] .

Our lungs expand to intake atmospheric air and contract to exhaust gasses created by metabolism back to the atmosphere. However, the lungs themselves do not have any muscles. Instead, the process relies on a simple physical principle known as **Boyle's law**. Our lungs are located in a cavity inside the chest, known as the *thoracic cavity*. As the volume of the thoracic cavity increases, it creates low pressure inside the lungs. This low pressure forces the atmospheric air into the lungs. Similarly, as the volume of the thoracic cavity decreases, it creates high pressure inside the lungs, which forces the air out back to the atmosphere.

The expansion of the thoracic cavity mainly depends on the diaphragm and *intercostal muscles*, a group of small muscles located between ribs. These muscles are shown in Figure 11. While breathing quietly, most of the expansion comes from the diaphragm, and intercostal muscles also take part in the process. Expiration, however, normally depends on muscle flex alone. There are other muscles that are also associated with respiration, known as *accessory muscles*. These muscles are not used for regular breathing. However, forced breathing may utilize these muscles both for inspiration and expiration[28].

Respiration has several modes. The first mode is called *forced breathing*,

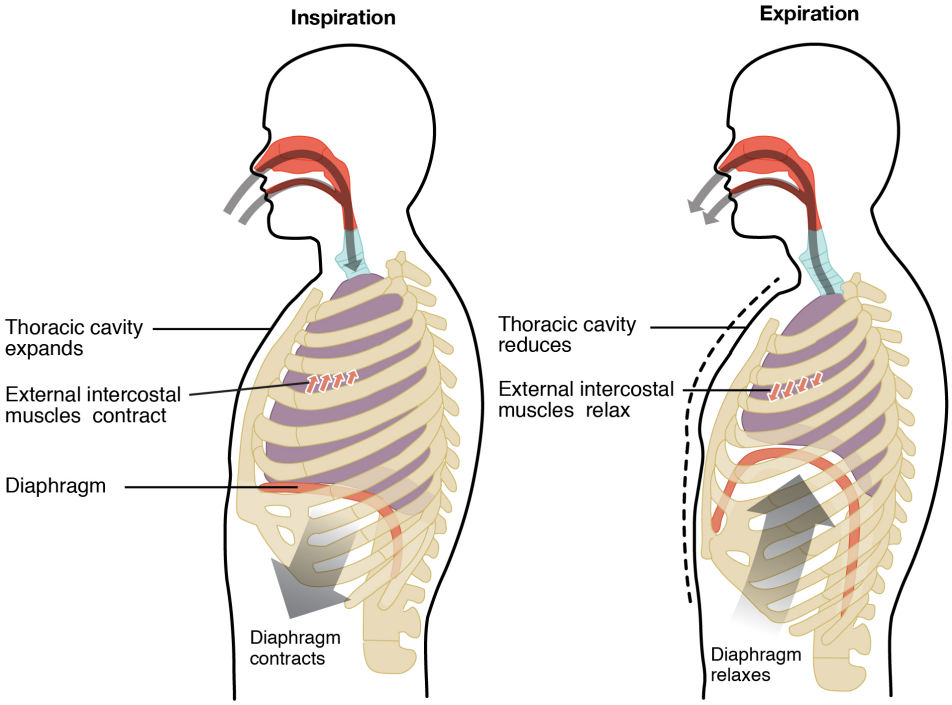

Figure 11: Figure showing thoracic cavity volume and associated muscles. The left image shows inspiration, with a contracted diaphragm and intercostal muscles and increased lung volume. The right image shows expiration, with a relaxed diaphragm and intercostal muscles and decreased lung volume. Source: [28]

and it is used when the person needs better control of breathing. This applies to cases such as singing and exercising. The second mode is called *quiet breathing*, and it happens without cognitive thought. This mode applies to normal breathing as well as breathing at rest. Since the intention of this thesis is to estimate the respiration rate for sleep monitoring, we will only assume quiet breathing for our analysis.

It is also possible to divide quiet breathing into two sub-modes: One of them is called *deep breathing*, or *breathing into the stomach*, or *diaphragmatic breathing*. The other one is called *shallow breathing*, or *chest breathing*. The difference between these styles is the involvement of the diaphragm. Deep breathing utilizes both diaphragm and intercostal muscles, while shallow breathing only utilizes intercostal muscles. As a result of this, the thoracic cavity expands more with deep breathing, allowing for more air exchange.

2.3 Autocorrelation Function

Autocorrelation function (ACF) is a mathematical operation used for seeing how the signal correlates with itself over time. In other words, it tells how it repeats itself over time. An effect of this operation can be seen in Figure 12.

In this thesis, we used ACF to determine the repetition interval of the respiration signal. Even though it is a mathematically complicated operation, it is very easy to understand by looking at the plots of input signals and the output signal. In this section, we will discuss ACF by starting from the convolution operation and how it processes signals. We will do so by starting from the mathematical description and then continue with plots to also give a graphical explanation. Later, we will define ACF using convolution.

2.3.1 Convolution

Convolution is a mathematical operation also used in many practical applications. From a broad perspective, it tells how a function behaves when another function is applied to it. For example, it allows us to calculate airplane wing behavior under extreme conditions without going through expensive trial-and-error iterations [41]. As another example, convolution is used by a group of scientists and artists to create an album reenacting how Hagia Sophia might have sounded like during a Byzantine mass [38]. They were able to create it by popping balloons inside the building to obtain the impulse response of the acoustic system, and they convoluted their studio-recorded mass with this impulse response to get the effect.

Coming back to mathematics, the convolution operation $*$ is defined as

$$(f * g)(t) = \int_{-\infty}^{\infty} f(\tau)g(t-\tau)d\tau.$$

As we have discussed earlier, it can be easier to understand this operation by

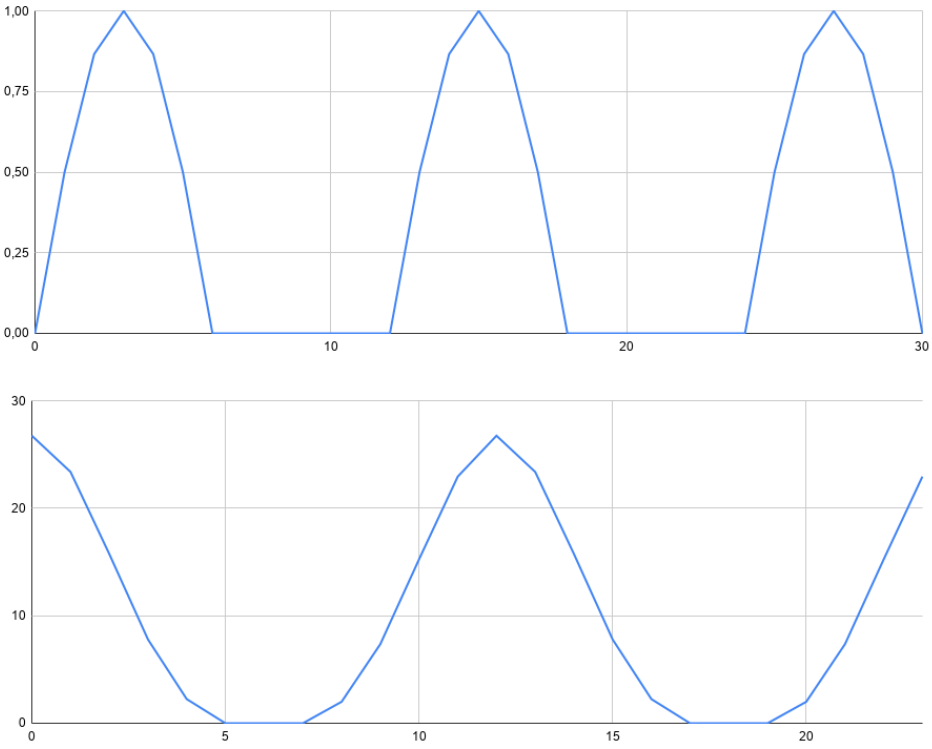

Figure 12: Top: Input signal, positive half of $sin(30x)$. Bottom: ACF of the input signal. Note that the ACF output has a visible peak at 0 and 12. This means that the input signal highly correlates with $sin(30(x+0))$ and $sin(30(x+12)$. In other words, it highly correlates with itself when it is not shifted and when it is shifted by 12 units.

looking at the process depicted in Figure 13. The same operation can also be defined for discrete signals as

$$(f * g)[n] = \sum_{m=-\infty}^{\infty} f[m]g[n-m].$$

2.3.2 ACF

Autocorrelation can be calculated by convoluting a function by itself. Mathematically it is defined as

$$(f * f)[n] = \sum_{m=-\infty}^{\infty} f[m]f[n-m]. \tag{4}$$

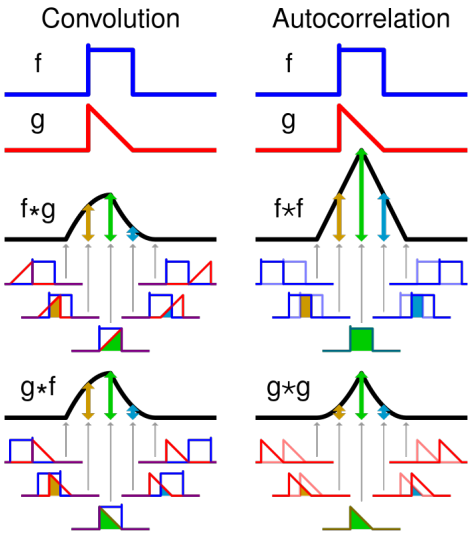

Figure 13: Both f and g are unit step functions. It is easy to visualize the operation by thinking f as stationary and g as moving. In this case, the integral calculates the intersection of two signals. Initially, there is no intersection. Therefore, the output of the convolution is zero. Later, both signals start to intersect, and the convolution ramps up until they both intersect completely. Right after that, convolution starts to ramp down as the shapes start to move away from each other, and then it reaches back to zero when they no longer intersect. Image from `https://commons.wikimedia.org/wiki/File:Comparison_convolution_correlation.svg`, created by Cmglee (Creative Commons, BY-SA)

Similarly to convolution, it is easier to understand it by looking at the plots, as can be seen in Figure 13.

3 Method

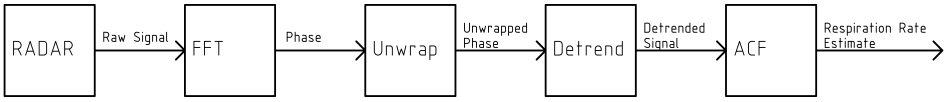

Figure 14: Block diagram showing the signal processing steps. More details about the raw signal and its processing using FFT can be found in Section 3.1. The unwrapping process is explained in detail in Section 2.1.4, and ACF in Section 2.3.2.

Breathing in and out causes movements on the torso and our method exploits this to estimate the breathing rate of an individual. We have achieved this by observing the chest movements with radar and processing the output signal using the blocks shown in Figure 14. In this chapter, we will be explaining the individual signal processing blocks as well as some of the design decisions behind them.

3.1 Raw Signal and FFT

The raw radar signal is the starting point of the estimation process. This signal is the *Intermediate Frequency* signal sampled by the microcontroller on the radar hardware. More on this can be found in Section 2.1.2.

Ideally, we expect this signal to be completely flat when there is no object in the range to reflect the transmitted signal. However, due to small crosstalk between the antennas, we get a non-zero signal even when the radar is pointed at the sky, with nothing in range for at least hundreds of meters. This effect can be seen in Figure 15.

On the other hand, as more reflective objects get closer to the radar, we see that the reflections start to dominate the crosstalk. The difference can be seen in the first plot of Figures 16 and 17. However, the raw signal is difficult to interpret visually. Thus, we apply FFT and get the signal shown in the second plots of Figures 16 and 17.

It can be seen more clearly in Figure 16 that there is an object near the second and third bins. If we approximate that the peak is located exactly at 2.5th bin, and multiply it with 0.6 meters, which is the resolution of this radar as discussed in more detail earlier in Chapter 2, we get a distance of 1.5 meters. If we do the same calculation for Figure 17 and assume that the peak is exactly at the 5th bin, then we get 3 meters of distance. Please note that the crosstalk is very dominant in the measurement done in Figure 17. For our application, the operation depicted in Figures 16 and 17 can be used to detect the presence, to see whether the bed is occupied or not. This step can also be used to detect the most useful FFT bin for the next step.

The experiments depicted in Figures 15, 16, and 17 show the radar's

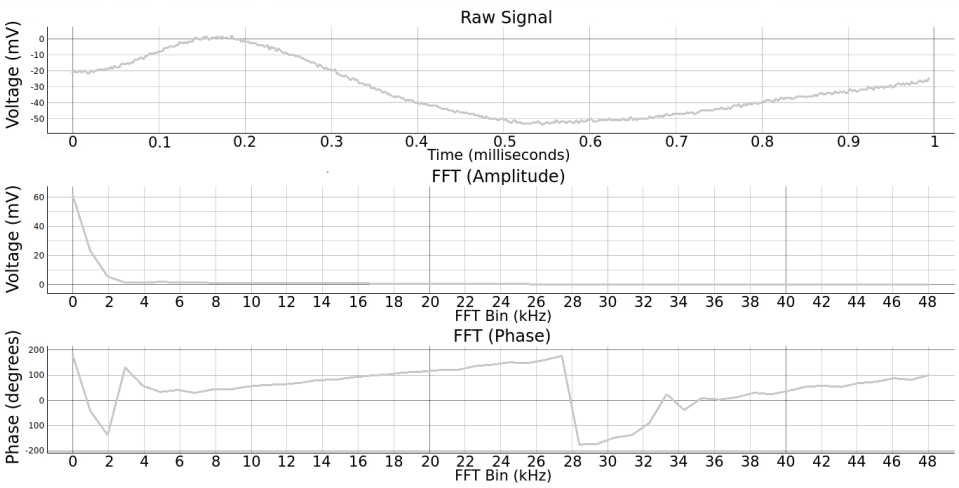

Figure 15: Radar output when it is pointing at the sky, with no visible target. Top: Voltage vs. time, showing the raw signal that comes out of the radar. Middle: Voltage versus FFT bin, showing the amplitude component of the FFT output. Bottom: Phase versus FFT bin, showing the phase component of the FFT output. Note the non-zero raw signal caused by the interferences between the antennae. Also note the strong strength of lower bins, signifying DC and low-frequency components in the raw data.

capabilities using one-shot data. On the other hand, we can also choose an FFT bin to track movements over time. This approach creates more useful data for our purpose of estimating the respiration rate. We have primarily used the average of 4^{th} bin and its neighbors within a range of 2 during our experiments. We have chosen these bins to avoid the DC component and also because of the small distance between the radar and the experiment subjects.

Although the amplitude component of FFT is useful for measuring the distance between the radar and the tracked object, we found it more useful to use the phase component to track small movements caused by respiration. A comparison can be found in Figure 18. The output signal of this step can be seen in Figure 19 for different cases.

3.2 Detrending

A curve that is fit over data is called a *trend*. For example, if we fit a line over a country's population per year, we get the population increase trend of that country. This gives information about the future of the data based on the current information. However, if we want to better observe sudden and small changes in the signal, then we need to remove the trend from the signal. This operation is called *detrending*. In SciPy, this operation is performed by

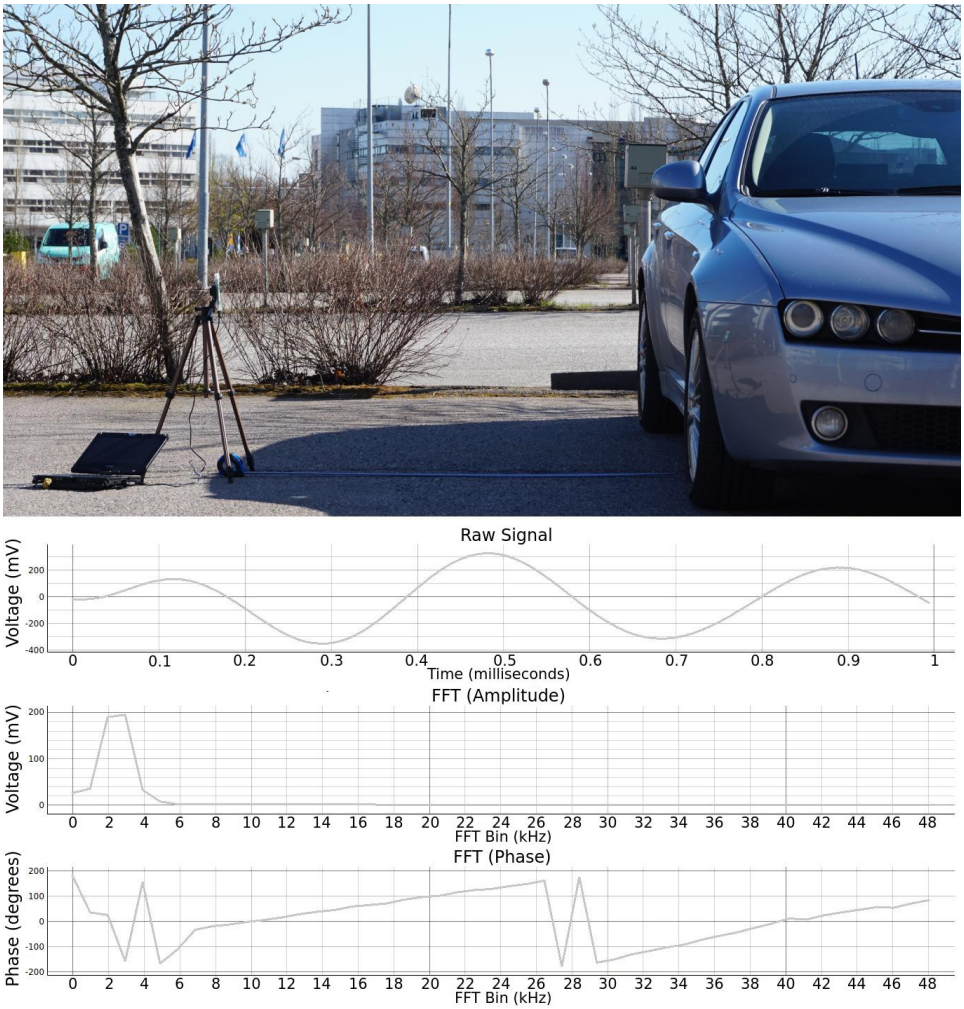

Figure 16: Figure showing the experiment setup and the measurement of a highly reflective object with the radar. In this case, the target (a car) is 1.5 meters away. From top to bottom: Experiment setup, voltage versus time graph showing the raw data, voltage versus FFT bin graph showing the amplitude component of the FFT, and phase versus FFT bin graph showing the phase component of the FFT. Note the bump on the FFT amplitude chart at the second and third bins. Also note that the FFT phase does not give any information when compared to Figure 15

detrend [15].

We use detrending in our application to have a more workable signal since the detrending operation moves the signal to the vicinity of the zero line as well as to eliminate slow movements of the signal caused by anything other than respiration. To elaborate, this operation ensures that the unwrapped

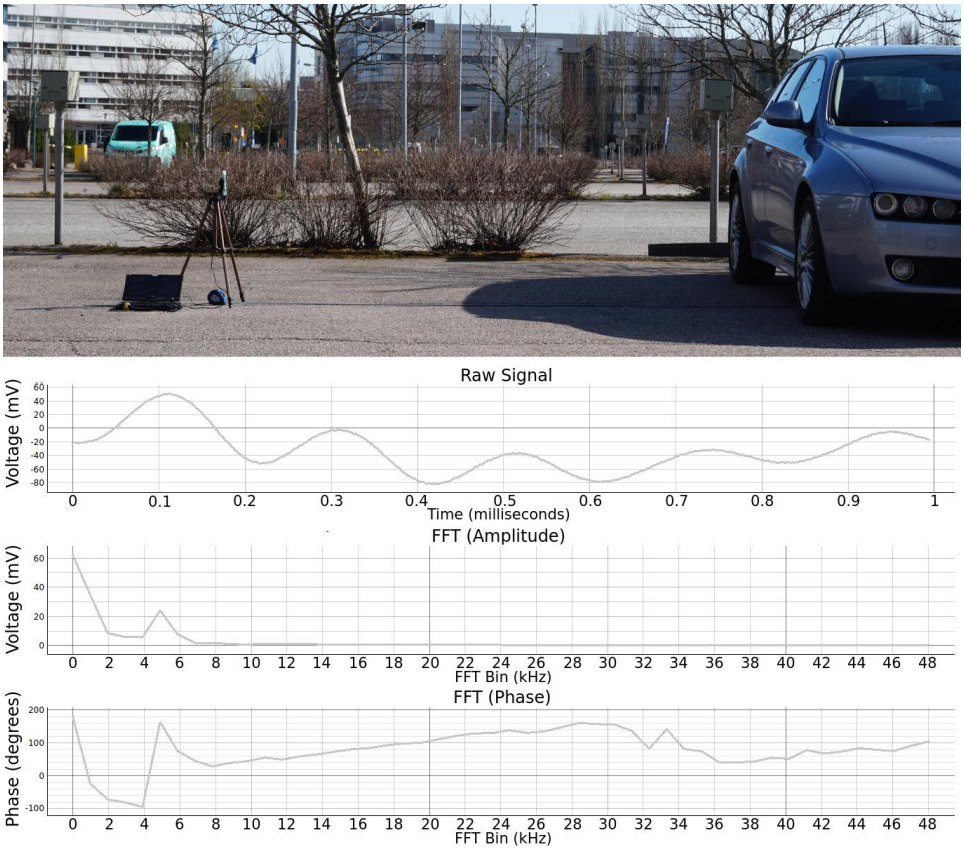

Figure 17: Figure showing the experiment setup and the measurement of a highly reflective object with the radar. In this case, the target is 3 meters away. From top to bottom: Experiment setup, voltage versus time graph showing the raw data, voltage versus FFT bin graph showing the amplitude component of the FFT, and phase versus FFT bin graph showing the phase component of the FFT. Note the bump on the FFT amplitude chart in fifth bin. Also note that the bump is smaller compared to Figure 16. This is a result of the distance on the received signal. Since the energy is low, the interference between the antennas (see Figure 15) has a strong influence, which appears closer to the zeroth bin.

signal always oscillates around the zero line. This helps to keep the signal interpretable since, occasionally, it is possible for the numbers behind the signal to climb up due to the unwrapping process. In those cases, it is difficult to see the small changes in big numbers, compared to working with small numbers. It also helps to keep the signal flat in case of slow movements of the person, which is necessary for a successful operation of ACF. In our experiments, the effects of detrending were minimal. Likewise, we expect these kinds of movements to happen seldomly during sleep. Therefore, it is

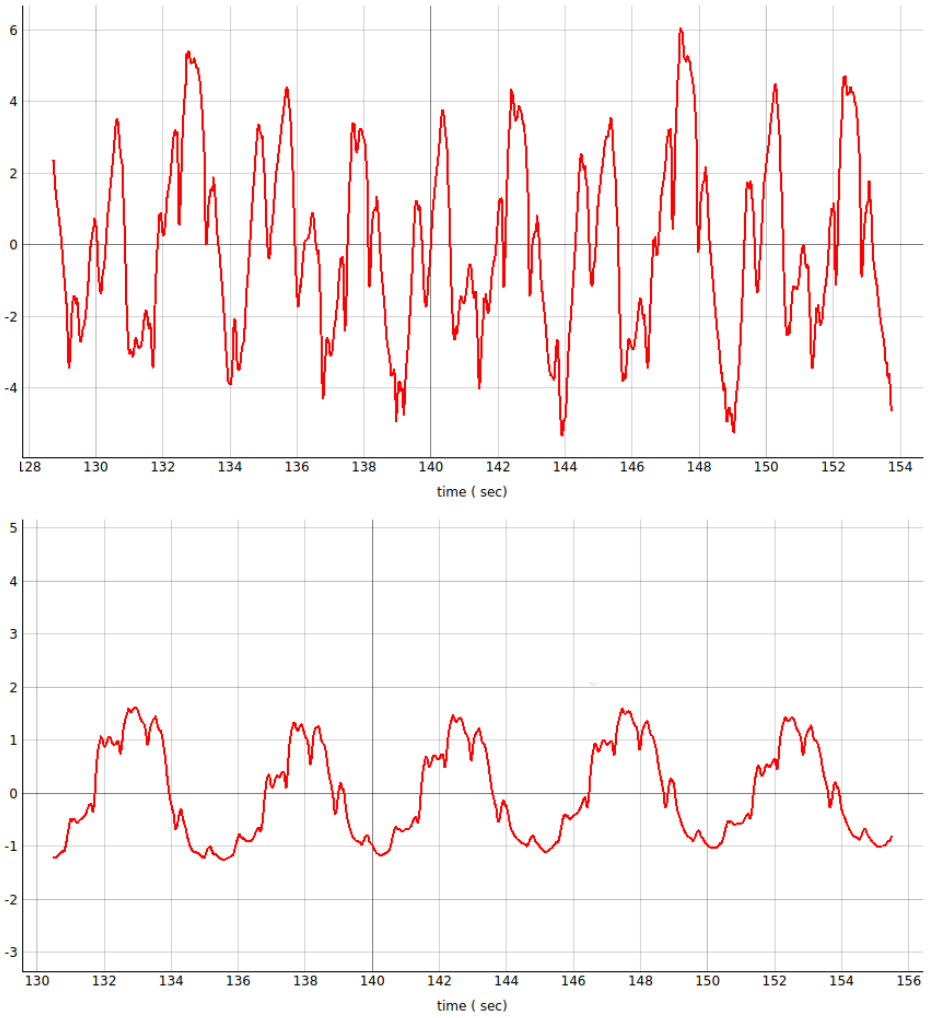

Figure 18: Figure showing the difference between observing amplitude and phase using the same dataset and same time window. The top plot shows the amplitude versus time plot, and the bottom plot shows the phase versus time plot. Note that the respiration rate for this dataset was approximately 12 cycles per minute, corresponding to 5 seconds between cycles.

possible to remove that step in order to conserve the computational budget without too much sacrifice in terms of performance. An effect of detrending can be seen in Figure 19.

3.3 ACF and Respiration Data

This is the part where we get the periodic signal in and output a number that is the estimation of the respiration rate. We have decided to use ACF, which

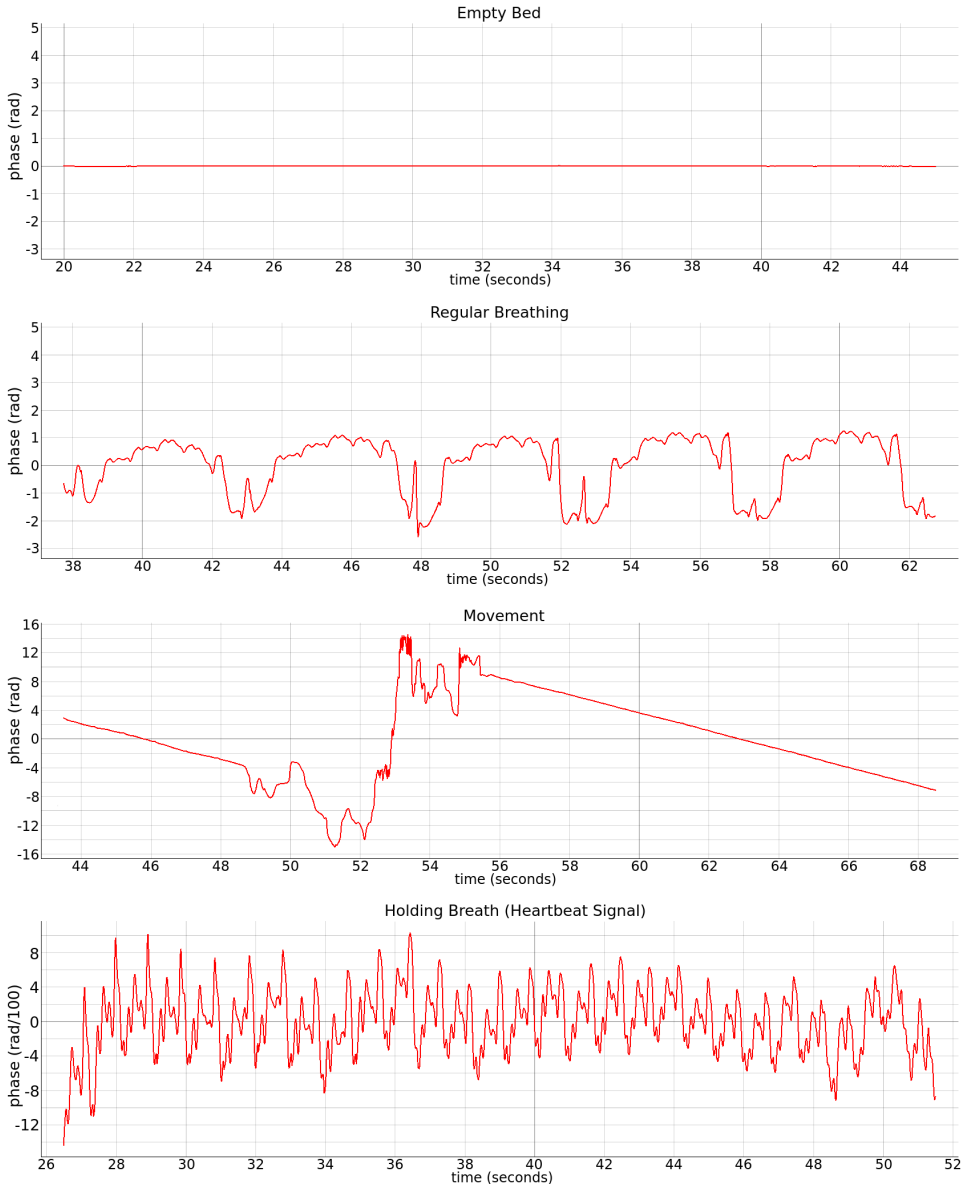

Figure 19: The figure shows multiple Phase vs. Time plots for different cases. From top to bottom, the first plot shows the case where there is no one in the bed. The second plot shows the curves created by regular breathing. Note the small bumps on the bigger signal created by heartbeats. The third plot shows when there is a big movement. In this case, this signal is created when the experiment subject was rotating to change his sleeping position. The slanted lines are an artifact of the detrending process. Fourth plot shows the heartbeat signals when the test subject holds his breath for a while.

is described in detail in Section 2.3.2, instead of using FFT. This decision was made because the FFT operation requires a far higher number of samples to get a decent resolution, which is especially important for observing changes in small frequency signals such as the respiration rate signal. Using Equation 2.1.3, we can calculate that we need approximately 80 seconds of sampling to get a resolution of approximately 0.7 respiration cycles per minute at 200 Hz sampling rate and an FFT size of 16384. On the other hand, we see from Equation (4) that the resolution of ACF operation is only $1/f_s$, where f_s is the sampling rate. This means that we can get good, consistent results using a buffer of 5000 samples, corresponding to 25 seconds of sampling.

4 Experiment Setup and Data

In this chapter, we will describe the experiment setup and discuss the data that we collected. We will start describing the physical experiment setup and the ground truth device, which is another vital sign measurement device that we used to compare our results against. Then we will describe the experiment process and briefly introduce the participants, as well as the goals of the experiment. Later, we will have a glance at a subset of the collected data and discuss the results.

Figure 20: A close-up of the experiment setup in Helsinki Think Company Viikki. Note that the field cot is just a piece of stretched cloth attached to the surrounding aluminum frame. The radar here is placed ground, under the field cot.

4.1 Experiment Setup

The first challenge is to design a measurement setup that resembles the real use cases, allowing a controlled experiment to be conducted at the same time. Since the outcome of this thesis is intended to be used to develop a sleeping sensor for babies, we wanted to simulate a sleeping setup. Thus, we have conducted the experiment on subjects whilst they were lying down. Moreover, we have chosen a bed, a foldable field cot, which resembles a hammock-type baby cot such as Lullame Solina [9] or Breathe Easy Baby Crib Mattress [4]. We have targeted this kind of mattresses partially because

of a possible future collaboration with Lullame, but also for practical reasons: We can place the sensor underneath the bed, as can be seen in Figure 20, and minimize the potential vibrations during our experiments. An alternative could be to hang the radar over the bed or on the ceiling. However, this would induce vibrations due to the swinging motion of the hanging apparatus or even by the people who walk on the top floor. On top of that, it would make the experiment setup less portable.

Apart from the radar, we have used a Zephyr BH3 sensor to obtain ground truth data from the participants. This device is mainly designed for monitoring and improving the training quality of physically active professionals, such as athletes, military personnel, and first responders [17]. However, since it also provides an API to interact with, it is also useful for non-medical research use.

The sensor can measure heart rate, heart rate variability, and respiration rate physiologically, and it features an onboard accelerometer. The device also allows more data to be derived by interpreting or combining these measurements, such as training intensity and caloric burn [18].

Figure 21: Image showing a mannequin torso with a Zephyr BH3 sensor. This is shown as the correct way of wearing the sensor. Note the location of the breathing sensor and also note the bump created by the sensor pod. The shoulder belt was not available during the experiment. Source: [19]

The device is worn on the chest, as depicted in Figure 21. It measures the respiration rate using a pressure sensor attached to the harness [21]. It measures the pressure changes as the chest expands and contracts and interprets the respiration rate from this signal. Although this method is not the most accurate one, since it highly relies on correct placement and adjustment of the sensor as well as the breathing style of the wearer, as discussed in Section 2.2, we deemed that it is sufficient for our experiment.

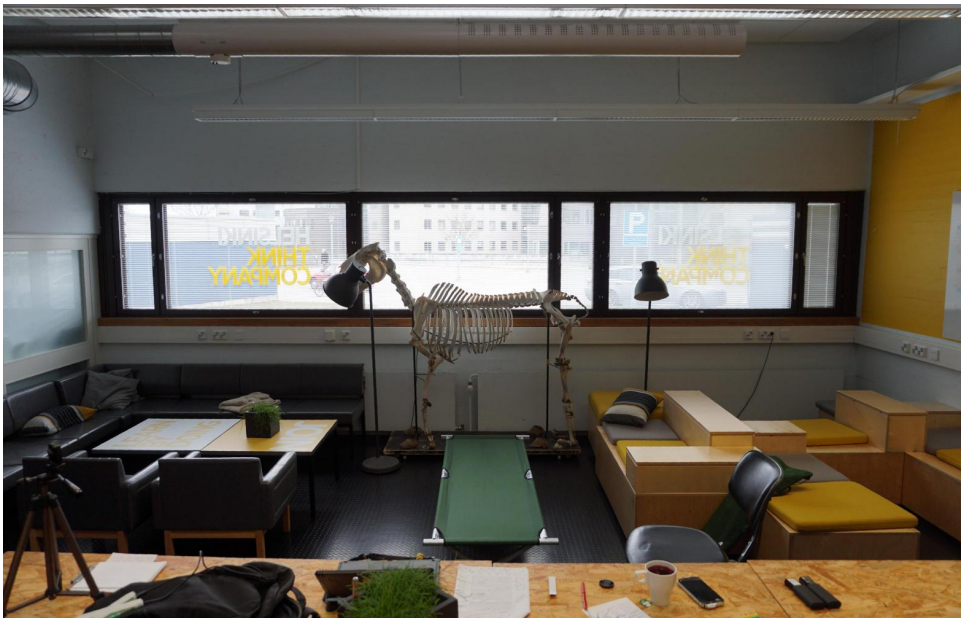

Figure 22: Location of the experiment: Helsinki Think Company premises located in Viikki. Note the field cot in the middle.

To further reduce external influences on the measurement, such as those caused by the environment, we used the same physical location and the same room to collect data from all the participants. The experiment location can be seen in Figure 22. Although this may sound insignificant, we thought that it is important since we are using radar, and the reflections of the signal could cause quality differences in the signal, resulting in differences between measurements.

4.2 Experiment Process

Since we wanted to simulate a sleeping environment, we requested our participants to lie on the bed during the experiment. Since we were not able to use babies as test subjects, we proceeded with adults. But we stuck to the possible real use cases for the rest of the experiment.

For example, in order to cover most of the poses one might take during their sleep, we took separate measurements in three different sleeping positions: while lying on their back, while lying on their right side, and while lying on their stomach. We have not included the case where they would be lying on their left side because, when correctly worn as shown in Figure 21, the main unit of the Zephyr BH3 would cause pain by applying pressure on the ribs. We believe that this decision does not affect the quality of the data since we are expecting the results to be similar to the case where the participants are lying on their right side.

Due to the limits of the radar and also to keep the interpretation process simple, we assumed deeper sleep states, and we assumed that there would be no movements other than those caused by heartbeat and respiration. Thus, we asked participants to stay still for approximately five minutes for each sleeping position.

We have also assumed following safe sleep guidelines, which recommend babies to sleep in the same room, but in their own cribs [14]. In other words, we assumed that there is only one person in the sensing range of the radar.

4.3 Participants and Goals of the Experiment

As mentioned in Chapter 1, this thesis is derived from an effort to use radar as a potential tool to estimate the breathing rate. Although the idea of using radar to extract breathing rate was originally intended to be used in a baby product, we have conducted our experiments only on adults. This decision was made because it is not practical to go through the necessary permission process of the University of Helsinki for a master's thesis. However, we believe that the same process described in this thesis will also work on babies, but it requires more careful planning for important ethical considerations.

In the meanwhile, we wanted to choose the experiment participants as diversely as possible to ensure that this study is realistic and comprehensive for the potential use case. The importance of diversity can be understood based on Section 2.2. To briefly summarize, different people have different breathing styles. For example, some people practice *diaphragm breathing*, which is also known as *breathing into the stomach*. However, some others utilize their diaphragms less. We expect this difference to cause an effect on the radar signal. Similarly, research shows that people have different breathing habits based on their sex [33] and lifestyle [43].

To account for these differences, we conducted experiments on multiple people from different backgrounds. The original plan was to include more participants to minimize the positive or negative bias of various externalities when we began data collection in March 2020. However, Covid-19 pandemic interrupted the data collection process, and we could experiment only on 7 participants, as illustrated in Table 2.

4.4 Data

Due to the current situation caused by the pandemic [32], the original data collection plan could not be fully implemented. As a result of that, we will be presenting the available data here as well as all the problems associated with it.

To better analyze the limited amount of data we could collect, we will present the data based on the quality of the data collection process. We will start with the case where the participants followed the procedure, and the

Participant No	Sex
1	M
2	F
3	M
4	M
5	F
6	M
7	M

Table 2: A list of participants

ground truth device worked flawlessly. Then, we will investigate the failure modes associated with Zephyr BH3, and finish with a few examples of radar measurement failures, mostly due to the motion of the test subject or of the test equipment.

Before starting with the details of the measurements, we see it necessary to explain the figures. The figures explained in this chapter contain a combination of radar data and ground truth data. To better compare them, we plotted them on the same chart, and therefore it is vital to understand the difference between the data points. In these figures, the *FMCW radar ACF estimate* is the radar estimation. We have two estimations made by Zephyr BH-3: The *standard estimate* and the *beat-to-beat estimate*. The difference between them is that the beat-to-beat estimate is calculated by measuring the time difference between captured breathing events. The standard estimate, however, is a slightly filtered version of this. In other words, we expect the beat-to-beat estimate to be instantaneous, while the standard estimate to be more smoothened. Unfortunately, the details of the smoothing operation are not specified by the manufacturer, but from its behavior, we believe it is based on moving average.

4.4.1 Perfect Data

As described in Section 4.1, Zephyr BH3 needs to be worn in a very specific way. This requirement roots from the way it measures vital signs. It uses a pressure sensor to measure the breathing rate [21]. This operation requires the sensor to be worn low enough on the chest, so more of the chest movement is available, but also high enough on the chest, so there is enough firmness underneath. Moreover, the belt tension should be adjusted carefully for the body type, so the sensor has just the right amount of pressure range to detect the respiration, and it also has enough friction so that it does not move away from the correct position.

The *perfect data* consists of correctly worn Zephyr sensor, as well as adhering to the experiment procedure described in Section 4.2. In other words, *perfect data* is the outcome of the experiment when everything goes

according to the plan. In this section, we will be demonstrating two of such cases.

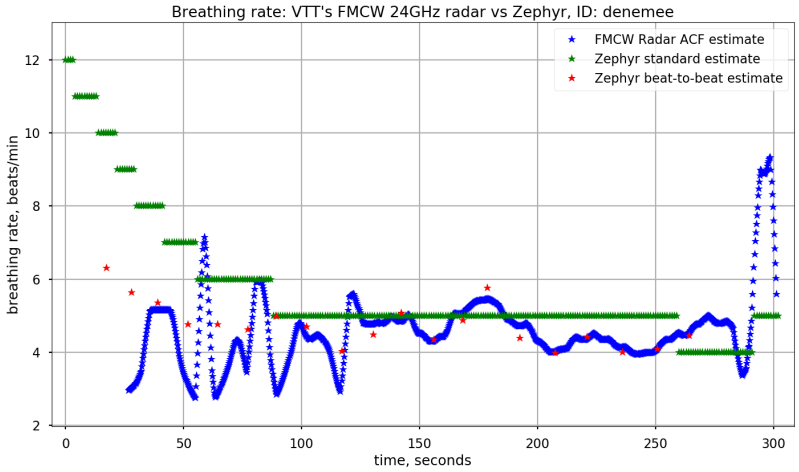

Figure 23: Comparison of the ground data with the radar estimations for subject 7 while lying on his back. Note that initially, the test subject shows other movements, confusing the radar estimate, but it stops at around 120 seconds mark. Also note that the instantaneous Zephyr data is lost somewhere around 270 seconds mark.

Subject 4 and Subject 7 The data presented here belong to subjects 4 and 7. What makes these two subjects special is the high availability of the instantaneous Zephyr breathing estimates. The availability of this information enables us to compare the accuracy of the radar with the ground data.

Each set of measurements are explained in their respective caption. This paragraph aims to guide the reader to the correct set of charts for a better understanding of the analysis.

Figures 23 and 24 show the measurement data from subject 7 while he is lying on his back and lying on his stomach, respectively. These data show how the radar would perform under more realistic conditions, i.e., in a deeper sleep state with a more steady breathing rate.

Figures 25 and 26 show the measurement data from subject 4 while he is lying on his side. Although both of these figures are taken from the exact same measurement setup, they demonstrate the effect of a design assumption. As mentioned in Section 4.1, we assumed a sleeping state during the experiment where the user would have minimal motion and steady breathing. However, this participant demonstrated high variability in his breathing regime. As a result of this, the estimation in Figure 25 shows a very poor fit. It is possible

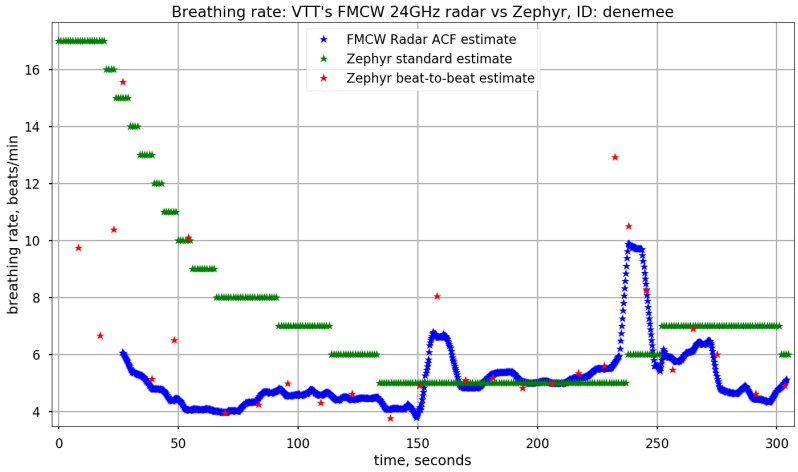

Figure 24: Comparison of the ground data with the radar estimations for subject 7 while lying on his stomach. The radar estimation and the instantaneous Zephyr data match almost perfectly. Note that the radar estimation starts at around 30 seconds mark when there are enough data points for the FFT analysis. Also note that the Zephyr standard estimate seems to be based on the moving average.

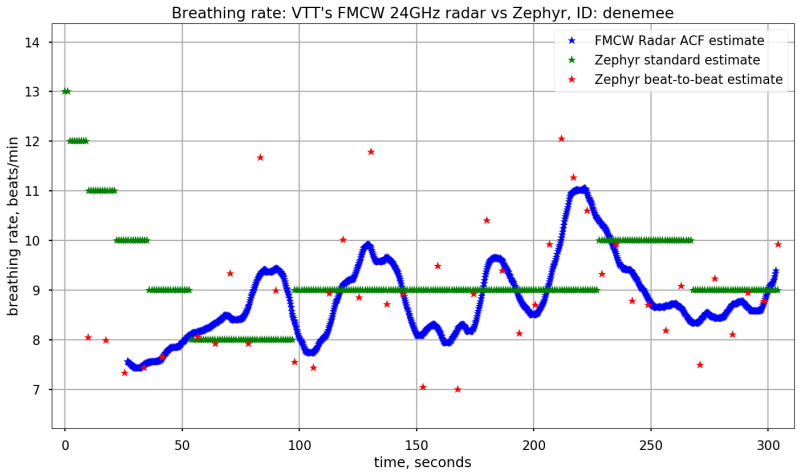

Figure 25: Comparison of the ground data with the radar estimations for subject 4 while lying on his side. An ACF buffer of 5000 data points is used. The radar estimation and the instantaneous Zephyr data match very poorly due to the averaging effect of bigger ACF buffer size

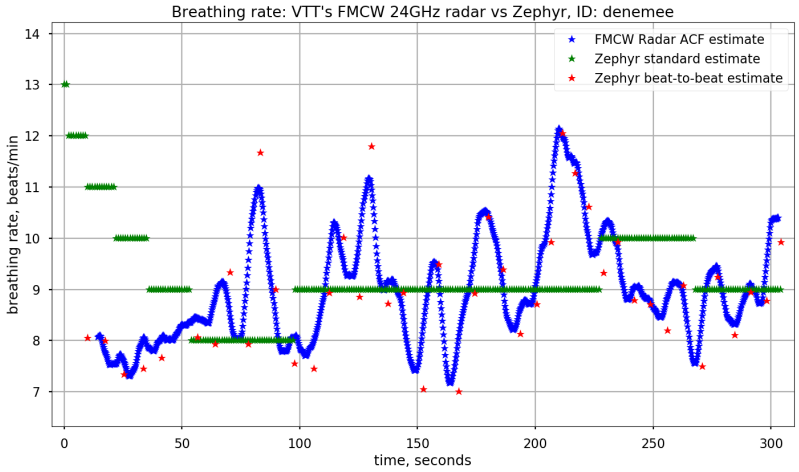

Figure 26: Comparison of the ground data with the radar estimations for subject 4 while lying on his side. An ACF buffer of 2500 data points is used. The radar estimation and the instantaneous Zephyr data match very closely despite the highly varying breathing rate thanks to a smaller ACF buffer size. Note that Zephyr standard estimate stays very stable.

to correct this by reducing the ACF buffer, defined in Section 2.3.2, and to get the close fit shown in Figure 26. Although this setting makes sensing more agile, it is not preferred since it causes unwanted jitter on the output data.

4.4.2 Zephyr BH3 Failures

Zephyr BH3 uses a pressure sensor to measure breathing rate [21]. This sensor, when the Zephyr BioHarness is worn correctly, is located on the left side of the chest, as shown in Figure 21. This method of measurement works nicely when the BioHarness is adjusted correctly. However, improper adjustment or incorrect positioning of the BioHarness causes measurement errors.

During our experiments, we found that the average breathing rate, labeled as *Zephyr standard estimate* in figures, is mostly reliable. In a few cases, it started high, but it reached the correct level later on. This can be seen, e.g., in Figure 24 and in some others as well. However, the instantaneous breathing rate, labeled as *Zephyr beat-to-beat estimate* in figures, has not been as reliable.

In this section, we will be studying the output data where the instantaneous breathing rate is not correct. In some cases, Zephyr BH3 reported lower instantaneous rates, but in some other cases, it reported no instantaneous

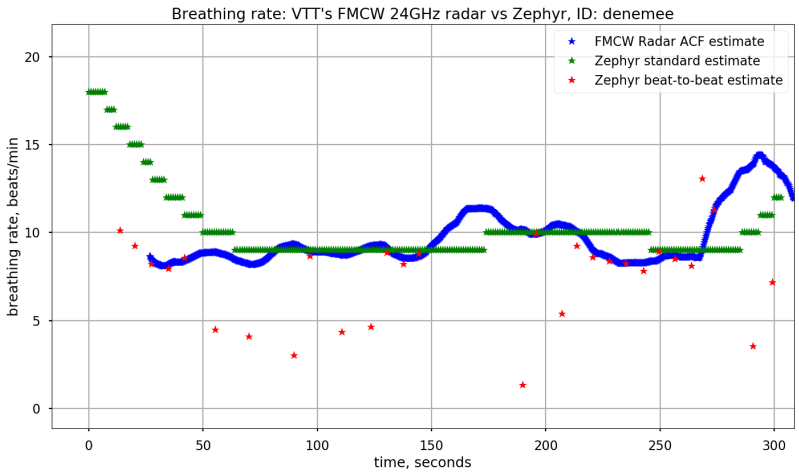

Figure 27: Comparison of the ground data with the radar estimations for subject 2 while lying on her stomach. Note that even though the instantaneous Zephyr data does not follow the radar estimation very closely, the radar estimation is very clean, and it follows the average Zephyr data. This indicates that radar estimation is valid. Also, the instantaneous Zephyr data fits very nicely between 210-260 second marks.

rates at all.

Similar to Section 4.4.1, each set of measurements are explained in their own caption. The following paragraphs are intended only to guide the reader to the right measurement figures.

Partial loss of instantaneous breathing rate Figure 27 shows the subject 2 while she is lying on her stomach, and Figure 28 shows the subject 6 while she is lying on her side. In both of the cases, instantaneous Zephyr data seems available, but it also seems that it is reporting less than normal. However, average Zephyr data still seems available, and it follows the radar estimation very closely.

Figure 28 shows some anomaly regarding the radar data. This will be studied further in Section 4.4.3

Complete loss of instantaneous breathing rate Figure 29 shows subject 5 while he is lying on his stomach, and Figure 30 shows subject 6 while she is lying on her stomach. In both of the cases, instantaneous Zephyr data is not available. However, average Zephyr data still seems available, and it follows the radar estimation very closely.

Figure 30 shows some anomaly regarding the radar data. This will be studied further in Section 4.4.3

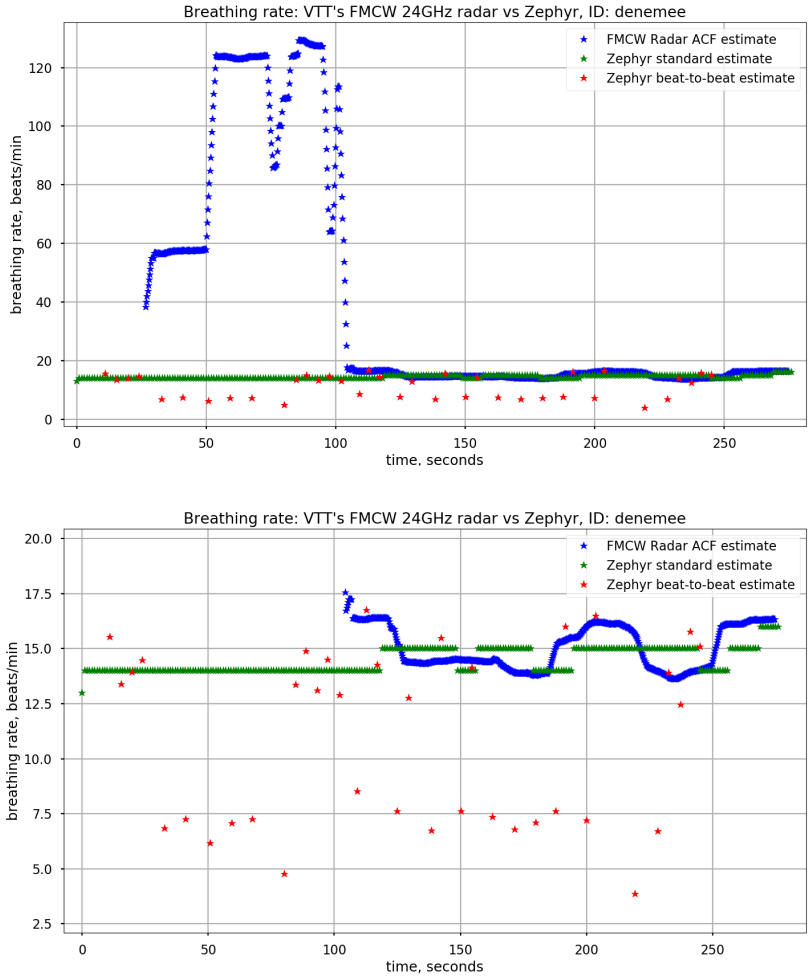

Figure 28: Comparison of the ground data with the radar estimations for subject 6 while lying on her side. The top graph shows all the data points. The bottom graph is vertically scaled to show more details of the region after 100 seconds mark. Note that the scale of the top graph is off because of a partially faulty radar measurement. However, the radar data returns back to normal around 100 seconds mark. After that, it can be seen that the radar data follows the average Zephyr data very closely. However, similar to Figure 27, Zephyr reports a lower instantaneous rate compared to both the radar and the average. Also, similar to Figure 27, the radar data is clean after 100 seconds mark, and it follows the average very well, indicating that the radar data is valid.

4.4.3 Radar Failures

During the process, we have noticed that estimating the breathing rate using the radar is very sensitive to movement, as expected. Any small movement

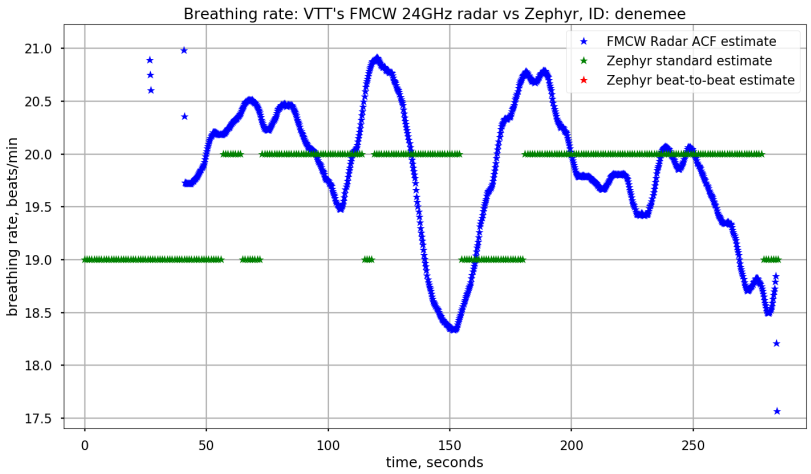

Figure 29: Comparison of the ground data with the radar estimations for subject 5 while he is lying on his stomach. Note that there is no instantaneous Zephyr data on the graph. However, the average Zephyr data is still available. Also note that the radar estimation appears very smooth, and it follows the average very closely. These features indicate that the radar data is valid.

of the subjects affects the radar data, and since it is usually bigger than those caused by breathing, it shadows the breathing data. In fact, bigger movements only create noise in the phase since the effects cause more change on the phase than π, resulting in an invalid phase unwrapping (see Section 2.1.4). In the end, ACF tries to pick repetitive features in the noise, and the radar estimate starts jumping around. It is not only the movement of the subject that throws the radar estimate off. Any nearby movement can also cause similar effects on the radar output. For example, it can be someone walking near the test setup. Unfortunately, this makes classifying the sources of errors very difficult.

However, we have also taken notes on participant behavior that can affect the radar data during the experiments. In one particular case, the test subject was slightly shaking his feet intermittently. The related data can be seen in Figure 31. In another case, the test subject was slightly moving himself to be more comfortable. This data can be seen in Figure 32.

The available cases demonstrate that invalid radar estimations can be picked out only by looking at the data. For example, consider the case shown in Figure 28. In this case, radar estimates a respiration rate close to 120, which is unrealistically high. We also expect a smoother breathing rhythm from a sleeping person. Therefore, sudden jumps may indicate faulty data. However, this could also be misleading. For example, consider Figure 24. In this case, there is a strong peak around 200 seconds mark. Visually, this

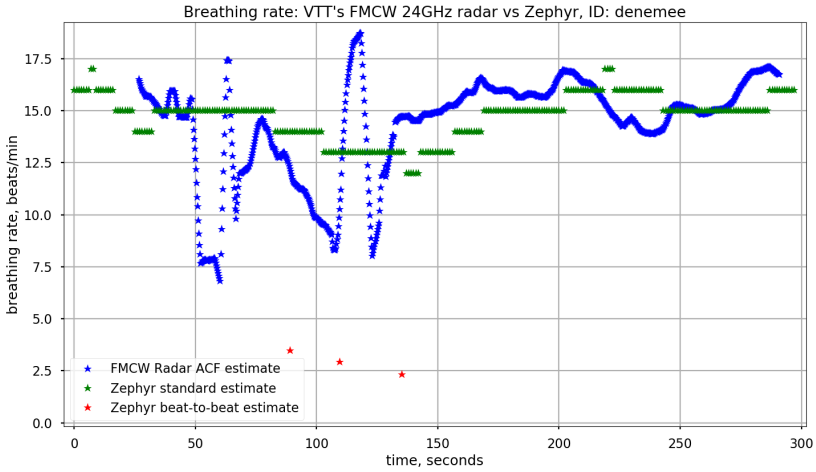

Figure 30: Comparison of the ground data with the radar estimations for subject 6 while she is lying on her stomach. Note that there are very few instantaneous Zephyr data, and they are very low. However, average Zephyr data is still available. Also note that the radar estimation is very rough until the 150 seconds mark, and it does not follow the average Zephyr data. This indicates that the radar data may not be valid. However, after 150 seconds mark, the radar estimation becomes smooth, and it follows the average Zephyr data very closely. This indicated that the radar data is valid.

appears as a sudden jump and, therefore, invalid. However, it appears valid since it is supported by the instantaneous Zephyr data.

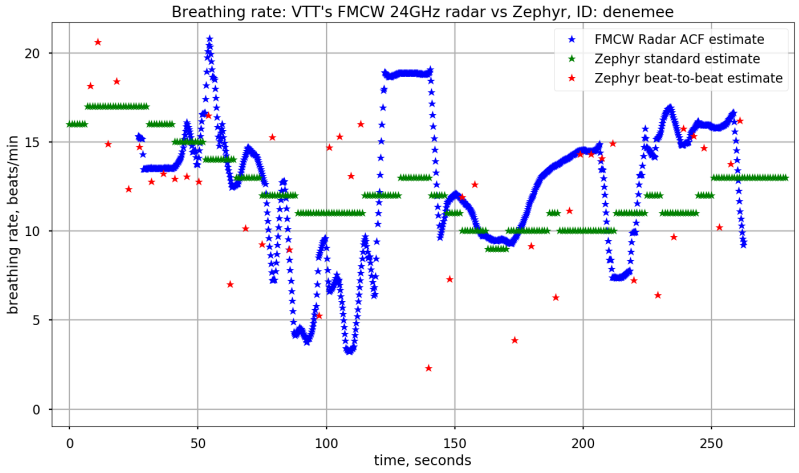

Figure 31: Comparison of ground data with the radar estimations for subject 3 while he is lying on his stomach. Note the extreme ups and downs of the radar estimate caused by foot shaking.

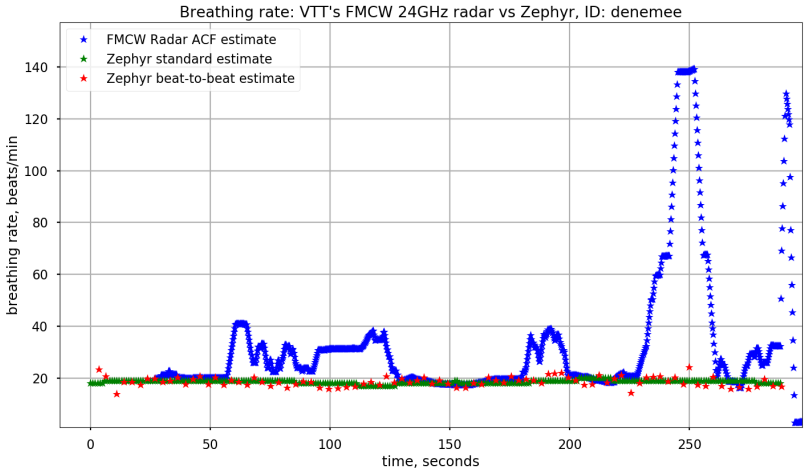

Figure 32: Comparison of ground data with the radar estimations for subject 5 while he is lying on his side. Note that the radar occasionally reports higher estimates than measured ground truth data.

5 Conclusions

We have described a complete system to measure respiration rate and compared it against a known off-the-shelf activity tracker that also measures respiration rate. Our experiments showed that our system could estimate respiration rate as good as the Zephyr BH3, our choice of off-the-shelf activity tracker while the users are lying on a bed or a mattress.

The advantage of our system is that it does not require the user to wear any electronic devices. Our system also provides users with the freedom of sleeping positions. In other words, our system does not require users to sleep in a certain position. One drawback of our system, however, is that it is not resilient to bigger movements while measuring the respiration rate. This was an expected result since we are using movement to estimate the breathing rate, and small signals cannot be detected due to the presence of a bigger signal. Bigger movements were expected to shadow smaller movements caused by breathing.

The human body acts differently depending on the sleep state. Respiration rate and heart rate vary depending on the sleep state. Likewise, the deeper the sleep movement, the more relaxed muscles are [3]. Therefore, we can use the drawback in our favor. Our observations showed that it might be possible to distinguish a big movement from respiration data. Therefore, it may be possible to classify data as *clean* and *movement*. In other words, our approach can provide useful input for sleep quality estimation, both using the actual respiration data and also the big movement data. However, since the scope of this thesis is limited to acquiring the respiration rate using an FMCW radar, this is left as a further study.

Other challenges related to the application of this system is the human factor. Since the radar operates at a high frequency, we expect the general public to be cautious against it. Similar reactions to high-frequency radio devices have been vocalized in different contexts. For example, a similar and popular concern is that 5G is linked to cancer, or it spreads coronavirus [39]. Even though these claims are not true, the aspect has to be takein into account.

To finalize, our experiment proved that an FMCW radar has a big potential for estimating the respiration rate as good as a commercial wearable sensor. But it requires additional work to address several technical and practical aspects. On top of that, we believe that the movement data can also be used as a data point for estimating sleep state. Also, the relevant research shows that it is possible to use all this data for measuring sleep quality, reinforcing the possibility of using an FMCW radar as a sleep sensor.

References

[1] *Beddit sleep sensor.* https://www.beddit.com/. Accessed: 2020-09-30.

[2] *Beddit sleep sensor faq.* https://www.beddit.com/faq/. Accessed: 2020-10-01.

[3] *Brain basics: Understanding sleep.* https://www.ninds.nih.gov/Disorders/Patient-Caregiver-Education/Understanding-Sleep#2. Accessed: 2020-10-25.

[4] *Breathe easy baby crib mattress.* https://bebsleep.com/product/breathe-easy-baby-crib-mattress/. Accessed: 2020-04-25.

[5] *Cpsc safety alert: Infants can strangle in baby monitor cords.* https://www.summerinfant.com/SummerInfant/media/SI_ProductManuals/Alert%20PDF/CPSC-Monitor-Power-Line-Cord.pdf. Accessed: 2020-10-11.

[6] *Guidesense - a wearable device for the visually impaired.* http://guidesense.com/en/. Accessed: 2020-10-25.

[7] *Guinness world records: Farthest distance travelled by a human voice.* https://www.guinnessworldrecords.com/world-records/farthest-distance-travelled-by-a-human-voice, Accessed: 2020-10-01.

[8] *Keep me safe! here's what to know for baby safety month 2018.* https://onsafety.cpsc.gov/blog/2018/08/31/keep-me-safe-heres-what-to-know-for-baby-safety-month-2018/. Accessed: 2020-10-11.

[9] *Lullame solina 2 in 1 - automated rocking and airy mattress for cot.* https://www.lullame.com/products/self-rocking-baby-mattress. Accessed: 2020-04-25.

[10] *Nanit smart baby monitoring system.* https://www.nanit.com/. Accessed: 2020-10-18.

[11] *Nomenclature of the frequency and wavelength bands used in telecommunications.* https://web.archive.org/web/20131031020427/http://www.itu.int/dms_pubrec/itu-r/rec/v/R-REC-V.431-7-200005-I%21%21PDF-E.pdf.

[12] *numpy.unwrap - numpy manual.* https://numpy.org/doc/stable/reference/generated/numpy.unwrap.html, Accessed: 2020-10-04.

[13] *Owlet smart sock baby monitor.* https://owletbabycare.co.uk/products/owlet-smart-sock. Accessed: 2020-10-18.

[14] *Safe sleep: Recommendations.* https://www.aap.org/en-us/advocacy-and-policy/aap-health-initiatives/safe-sleep/Pages/Safe-Sleep-Recommendations.aspx. Accessed: 2020-10-25.

[15] *scipy.detrend - scipy reference guide.* https://docs.scipy.org/doc/scipy/reference/generated/scipy.signal.detrend.html, Accessed: 2020-10-04.

[16] *Small parts for toys and children's products.* https://www.cpsc.gov/Business--Manufacturing/Business-Education/Business-Guidance/Small-Parts-for-Toys-and-Childrens-Products/. Accessed: 2020-10-11.

[17] *Zephyr components.* https://www.zephyranywhere.com/. Accessed: 2020-04-25.

[18] *Zephyr data.* https://www.zephyranywhere.com/benefits/physiological-biomechanical. Accessed: 2020-04-25.

[19] *Zephyr bioharness 3 user manual.* https://www.zephyranywhere.com/media/download/bioharness3-user-manual.pdf, September 2012. Accessed: 2020-05-24.

[20] *Wearables: 10 trends to watch.* Technical report, Tractica, 2015. https://www.tractica.com/resources/white-papers/wearables-10-trends-to-watch/.

[21] *Zephyr bioharness 3 log data descriptions.* https://www.zephyranywhere.com/media/download/bioharness-log-data-descriptions-07-apr-2016.pdf, April 2016. Accessed: 2020-04-25.

[22] Adib, Fadel, Mao, Hongzi, Kabelac, Zachary, Katabi, Dina, and Miller, Robert C.: *Smart homes that monitor breathing and heart rate.* In *Proceedings of the 33rd Annual ACM Conference on Human Factors in Computing Systems*, CHI '15, page 837–846, New York, NY, USA, 2015. Association for Computing Machinery, ISBN 9781450331456. https://doi.org/10.1145/2702123.2702200.

[23] Amit Kumar, Ms. Nidhi: *Radar pulse compression technique for linear frequency modulated pulses.* International Journal of Engineering and Technical Research (IJETR), Aug 2015. https://www.erpublication.org/published_paper/IJETR032817.pdf.

[24] Browne, Jack: *Pulsed vs. cw signals: Both loom on a designer's radar.* https://www.mwrf.com/technologies/systems/article/21849213/pulsed-vs-cw-signals-both-loom-on-a-designers-radar. Accessed: 2020-10-25.

[25] Cesar Iovescu, Sandeep Rao: *The fundamentals of millimeter wave sensors.* Technical report, Texas Instruments, 2017. http://www.ti.com/lit/wp/spyy005/spyy005.pdf.

[26] Chung, Gih Sung, Choi, Byung Hoon, Lee, Jin Seong, Lee, Jeong Su, Jeong, Do Un, and Park, Kwang Suk: *Rem sleep estimation only using respiratory dynamics.* Physiological measurement, 30(12):1327–1340, January 2009, ISSN 0967-3334.

[27] Gu, Changzhan and Li, Changzhi: *Assessment of human respiration patterns via noncontact sensing using doppler multi-radar system.* Sensors (Basel, Switzerland), 15:6383–98, March 2015.

[28] J. Gordon Betts, Kelly A. Young, James A. Wise Eddie Johnson Brandon Poe Dean H. Kruse Oksana Korol Jody E. Johnson Mark Womble Peter DeSaix: *Anatomy and Physiology.* OpenStax, Houston, Texas, Apr 2013. https://openstax.org/books/anatomy-and-physiology/pages/22-3-the-process-of-breathing, Accessed: 2020-10-24.

[29] Jardak, S., Alouini, M., Kiuru, T., Metso, M., and Ahmed, S.: *Compact mmwave fmcw radar: Implementation and performance analysis.* IEEE Aerospace and Electronic Systems Magazine, 34(2):36–44, Feb 2019, ISSN 1557-959X.

[30] Kiuru, T., Metso, M., Jardak, S., Pursula, P., Häkli, J., Hirvonen, M., and Sepponen, R.: *Movement and respiration detection using statistical properties of the fmcw radar signal.* In *2016 Global Symposium on Millimeter Waves (GSMM) ESA Workshop on Millimetre-Wave Technology and Applications*, pages 1–4, 2016.

[31] Lee, Jung Min, Byun, Wonwoo, Keill, Alyssa, Dinkel, Danae, and Seo, Yaewon: *Comparison of wearable trackers' ability to estimate sleep.* International journal of environmental research and public health, 15(6):1265, Jun 2018, ISSN 1660-4601. https://pubmed.ncbi.nlm.nih.gov/29914050.

[32] Liu, Yen Chin, Kuo, Rei Lin, and Shih, Shin Ru: *Covid-19: The first documented coronavirus pandemic in history.* Biomedical Journal, 43(4):328 – 333, 2020, ISSN 2319-4170. http://www.sciencedirect.com/science/article/pii/S2319417020300445.

[33] LoMauro, Antonella and Aliverti, Andrea: *Sex differences in respiratory function.* Breathe, 14(2):131–140, 2018, ISSN 1810-6838. https://breathe.ersjournals.com/content/14/2/131.

[34] Lusis, Dennis J.: *Hf propogation, the basics.* QST, Dec 1983. http://www.arrl.org/files/file/Technology/tis/info/pdf/8312011.pdf.

[35] O'Donnell, Dr. Robert M.: *Radar systems engineering.* http://radar-course.org/radar%20se%20List%20of%20Lectures%20.html. Accessed: 2020-10-25.

[36] Oppenheim, Alan V. and Schafer, Ronald W.: *Discrete-Time Signal Processing.* Prentice Hall Press, USA, 3rd edition, 2009, ISBN 0131988425.

[37] Pearce, J.M.S.: *A brief history of the clinical thermometer.* QJM: An International Journal of Medicine, 95(4):251–252, April 2002, ISSN 1460-2725. https://doi.org/10.1093/qjmed/95.4.251.

[38] Pentcheva, Bissera and Abel, Jonathan: *Icons of sound: Auralizing the lost voice of hagia sophia.* Speculum, 92:S336–S360, October 2017.

[39] Pressman, Aaron: *Does 5g cause or spread the coronavirus? here's what experts say.* https://fortune.com/2020/04/07/5g-coronavirus-health-cancer-radiation-studies-safely-use-cellphone/. Accessed: 2020-10-25.

[40] Rahman, Tauhidur, Adams, Alexander T., Ravichandran, Ruth Vinisha, Zhang, Mi, Patel, Shwetak N., Kientz, Julie A., and Choudhury, Tanzeem: *Dopplesleep: A contactless unobtrusive sleep sensing system using short-range doppler radar.* In *Proceedings of the 2015 ACM International Joint Conference on Pervasive and Ubiquitous Computing*, UbiComp '15, pages 39–50, New York, NY, USA, 2015. ACM, ISBN 978-1-4503-3574-4. http://doi.acm.org/10.1145/2750858.2804280.

[41] Silva, Walter A. and Branch, Aeroelasticity: *Identification of linear and nonlinear aerodynamic impulse responses using digital filter techniques*, Aug 1997. https://www.cs.odu.edu/~mln/ltrs-pdfs/NASA-97-tm112872.pdf.

[42] Skolnik, M.: *Introduction to Radar Systems.* McGraw Hill, 1979.

[43] Sukanya Badami, Mahesh Baragundi: *Effects of sedentary life style on respiratory rates and peak expiratory flow rate among medical students.* Indian Journal of Clinical Anatomy and Physiology, 4, 2020. https://www.ipinnovative.com/journals/IJCAP/article-full-text/3652.